Spring 4-19-2011

Functional Studies of Human Cellular Detoxification Enzymes

Melanie Neely Willis
University of Nebraska-Lincoln, melanieneelywillis@gmail.com

FUNCTIONAL STUDIES OF HUMAN CELLULAR DETOXIFICATION ENZYMES

by

Melanie M. Neely Willis

A DISSERTATION

Presented to the Faculty of

The Graduate College at the University of Nebraska

In Partial Fulfillment of Requirements

For the Degree of Doctor of Philosophy

Major: Biochemistry

Under the Supervision of Professor Joseph J. Barycki

Lincoln, Nebraska

May, 2011

FUNCTIONAL STUDIES OF HUMAN CELLULAR DETOXIFICATION ENZYMES

Melanie M. Neely Willis, Ph. D.

University of Nebraska, 2011

Advisor: Joseph J. Barycki

Cellular detoxification allows for the maintenance of cellular homeostasis and prevention of abnormal cell growth by clearing harmful xenobiotics and endobiotics. After oxygenation by phase I enzymes, phase II enzymes such as glucuronosyltransferases and glutathione-s-transferases conjugate a small molecule to the compound, marking it for subsequent export. Many up-stream enzymes are also essential to cellular detoxification by supplying the small compounds for conjugation. These up-stream enzymes include UDP-glucose dehydrogenase, which synthesizes UDP-glucuronate, and glutamate cysteine ligase, which catalyzes the first and rate-limiting step in the synthesis of glutathione.

UDP-glucose dehydrogenase (UGDH) is an important enzyme in human development and in the progression of many types of human epithelial cancers. Recently, mutations in UGDH were identified that are associated with congenital heart defects and cause a shift from a hexameric to a dimeric state. These clinical mutants, along with two engineered dimer mutants were used to examine differences in UGDH function resulting from loss of

hexameric structure. The dimer mutants exhibited near wild-type activity *in vitro*, and significant differences in UDP-glucuronate levels were not observed in HEK 293 cells. Despite this, the phenotype of development defects associated with the UGDH clinical mutants is at least partially explained by a reduction in protein stability.

Glutamate cysteine ligase (GCL) deficiency is a rare autosomal recessive trait that compromises production of glutathione, a critical redox buffer and enzymatic cofactor. Glutamate cysteine ligase is a heterodimer comprised of a catalytic (GCLC) and a regulatory subunit (GCLM). Four clinical missense mutations have been identified within GCLC: Arg127Cys, Pro158Leu, His370Leu, and Pro414Leu. Embryonic fibroblasts from GCLC null mice were transiently transfected with wild-type or mutant GCLC and cellular glutathione levels were determined to be significantly lower in the mutants relative to wild-type. In an *S. cerevisiae* model system, mutant GCLC alone could not complement a glutathione-deficient strain and required the concurrent addition of GCLM to restore growth. Kinetic characterizations of the recombinant GCLC mutants indicated that the Arg127Cys, His370Leu, and Pro414Leu mutants have compromised enzymatic activity that can largely be rescued by the addition of GCLM, while the Pro158Leu mutant has kinetic constants comparable to wild-type GCLC.

ACKNOWLEDGEMENTS

First, I would like to thank my advisor, Dr. Joseph J. Barycki, for his patient and thoughtful guidance these past years. I would also like to thank the members of my committee, Dr. Donald Becker, Dr. Mark Wilson, Dr. James Van Etten and Dr. Melanie Simpson for their ideas and contributions.

Next, I would like to thank the many members of the Barycki Lab, the Simpson Lab and the department of biochemistry who provided invaluable advice and support. I would particularly like to thank Ekaterina Biterova and Dharini Bharadwaj for teaching me so many things.

Finally, I would like to acknowledge the love and support of my friends and family. I thank my brilliant and devoted husband Stuart and my delightful son Aiden for making my years in graduate school happy and meaningful. I thank my parents, who have navigated the ebb and flow of life with grace and dignity.

Table of Contents

Chapter 1

Introduction

1.1 Cellular detoxification pathways

Cellular detoxification pathways are essential to the maintenance of cellular homeostasis and prevention of disease or progression of abnormal cell growth. Small hydrophobic molecules diffuse freely across the plasma membrane, allowing the entry of potentially harmful levels of xenobiotics or endogenous compounds into the cell. Fortunately, cellular detoxification is both efficient and broadly specific, allowing many different classes of compounds to be effectively cleared from the cell in a 3-step process [1, 2]. First, phase I enzymes (primarily members of the cytochrome 450 family of enzymes) oxygenate a compound, making it an appropriate substrate for phase II enzymes. These enzymes, which include glucuronosyltransferases and glutathione-s-transferases, conjugate a small molecule, such as glucuronate or glutathione, to the compound. These conjugated molecules mark the compound for subsequent export through multi-drug resistance transporters [1, 2].

Besides phase I and phase II enzymes, a multitude of up-stream enzymes participate in cellular detoxification by regulating the availability of small molecules for conjugation to xenobiotics. Thus, UDP-glucose dehydrogenase converts the common metabolite UDP-glucose into UDP-glucuronate, which may then be used as a substrate by UDP-glucuronosyltransferases (UGTs) or in glycosylation reactions in the lumen of the ER [3]. Besides participating in clearance of xenobiotics, UGTs also

glucuronidate endogenous compounds such as bilirubin and steroid hormones allowing them to be exported from the cell [4].

Similarly, glutathione has a variety of important cellular fates after sequential synthesis by glutamate cysteine ligase and glutathione synthetase. Glutathione's role as a redox regulator is well recognized [5, 6]. However, glutathione is also used extensively by glutathione-S-transferases to tag compounds for export and metabolize the by-products of oxidative stress [7]. The role of glutathione in cellular detoxification, like that of UDP-glucuronate, is especially critical in the liver, where the rate of detoxification is particularly high and a disproportionate amount of phase I, phase II, and upstream enzymes are synthesized [4].

Because of the critical roles of these two enzymes in supplying metabolites necessary for the detoxification of endobiotics and xenobiotics and their other cellular roles in metabolism and redox homeostasis, UDP-glucose dehydrogenase and glutamate cysteine ligase are ideal candidates for structural studies to reveal the basis of *in vivo* and *in vitro* enzyme function.

1.2 Roles of UDP-glucuronate

UDP-glucuronate is an important cellular metabolite utilized as a precursor in glycosaminoglycan synthesis, protein glycosylation, and cellular detoxification [8,10, 13]. UDP-glucuronate is synthesized from UDP-glucose by the enzyme UDP-glucose dehydrogenase via two successive oxidations to convert the 6′ hydroxyl to a carboxylate. UDP-glucuronate has a variety of

cellular fates, many of which involve further conversion at the ER or Golgi lumen [9].

UDP-glucuronate is incorporated into glycosaminoglycans in a variety of ways. The enzyme UDP-xylose synthase or UDP-glucuronate decarboxylase, located in lumen of the ER and Golgi, decarboxylates UDP-glucuronate to form UDP-xylose [10]. UDP-xylose is a precursor for the synthesis of these glycosaminoglycans: heparin, heparin sulfate, chondroitin sulfate and dermatan sulfate [9, 11]. UDP-glucuronate is also incorporated into hyaluronan, another glycosaminoglycan, that is synthesized at the cell surface and extruded into the extracellular space [8]. Glycosaminoglycans may function independently as cellular coating or connective tissue or may be attached to proteins in the late ER or Golgi [9]. Glycosaminoglycan synthesis has been implicated in developmental defects, cancer progression, arthritis, [12]and other disease states.

UDP-glucuronate contributes to protein glycosylation by providing glucuronosyl units and xylose units for sugar transferases. Several types of proteoglycans may be formed. Certain signaling proteins on the extracellular surface are O-glucosylated and xylosated [13]. An example of this is the xylosylation on O-glucose in EGF repeats on the Notch protein [10]. Additionally, synthesis of proteoglycans containing glycosaminoglycans in the late ER and Golgi are initiated by transfer of a core tetrasacharride containing xylose, two galactose units and a glucuronate to a serine in the protein [14,

15]. After transfer of this priming linker, glycosaminoglycan biosynthesis proceeds by addition of constituent sugars by sugar transferases.

Finally, UDP-glucuronate is the substrate for UDP-glucuronosyltransferases, arguably the most important class of the phase II drug metabolizing enzymes. Besides their critical role in detoxifying xenobiotics, UDP-glucuronosyltransferases also allow cells to remove toxic endobiotics [3, 4]. These enzymes attach the glucuronate moiety to the compound, allowing the conjugate to be exported by multi-drug resistance proteins in the plasma membrane. Thus, UDP-glucuronate is a cellular metabolite with essential roles in the synthesis of glycosaminoglycans and proteoglycans and in cellular detoxification.

1.3 UDP-glucose dehydrogenase

Human UDP-glucose dehydrogenase (UGDH) is an enzyme that catalyzes the conversion of UDP-glucose to UDP-glucuronate by two successive oxidation reactions. Much has been learned about the structure, function and regulation of UDP-glucose dehydrogenase through *in vitro* kinetic assays, x-ray crystallography and *in vivo* investigations.

The initial characterizations of UGDH were performed using *S. pyogenes* and bovine liver UGDH, both enzymes that have a high similarity to human UGDH. These early studies revealed a number of important features of UGDH function. First of all, while UGDH was thought to exist as a homo-hexamer in humans and higher organisms, studies suggested that the

hexamer contained only three active sites [16-18]. Also, it was recognized early on that a catalytic cysteine was essential for the reaction, though it was later realized that the cysteine is critical not in the first oxidation, but the second [19-22]. The roles of other active site residues have been clarified through mutagenesis, making possible the proposal of a reasonable reaction mechanism involving a first oxidation to a thiohemiacetal intermediate and further oxidation to a thioester intermediate before release of the product by hydrolysis [8, 20, 22, 23].

The determination of the first crystal structure of UGDH, the *S. pyogenes* structure, informed many of the kinetic mutagenesis studies. The later availability of the *C. elegans* and human structures has confirmed the close structural similarity of the human enzyme to the bacterial enzyme. The available crystal structures highlight an interesting feature of the enzymes that has been demonstrated by other methods as well: the bacterial enzyme is a dimer, while the human enzyme is a hexamer.

In vivo studies of UGDH have focused primarily on regulation of the enzyme at the transcriptional and post-translational levels, as well as, the involvement of UGDH in epithelial cancers and development abnormalities. UGDH is known to be transcriptionally up regulated in response to androgens in various tissue types, including the prostate epithelium and breast cancer cells [24-26]. It has also been shown that the UGDH promoter contains a peroxisome proliferative receptor α (PPAR α) response element that mediates

up regulation of UGDH in response to certain xenobiotics [27, 28]. At the post-translational level, UGDH activity responds to a variety compounds. UDP-xylose has long been recognized as an effective inhibitor of UGDH function [29]. A recent study also implicates two polyphenols, gallic acid and quercetin, in inhibition of UGDH activity in the cytosol [30].

UGDH has been associated with several pathological states in humans and other species. The production of UDP-glucuronate for use in production of extracellular-matrix polysaccharides impacts the progression of many types of human epithelial cancers, including prostrate, breast, head and neck, ventricle, colon, and pancreas cancer [31]. Additionally, several recent studies in related organisms indicate UGDH has a significant, but poorly delineated, role in development. The effects may be severe and cause embryonic lethality as is the case when the *sugarless* gene of *D. melanogaster* contains certain mutations [11] or less severe as is the case of mutations of the *sqv-4* gene of *C. elegans* that results in defects in vulval morphogenesis [32-34]. Mutation of the *jekyll* gene, which encodes UDP-glucose dehydrogenase, of zebra fish results in defects in heart valve formation [35]. These phenotypic developmental problems seem to stem from problems with the formation of proteoglycans and glycosaminoglycans, which require adequate levels of UDP-glucuronate precursors.

In conclusion, UDP-glucose dehydrogenase is an important enzyme in human development and in the progression of many types of human epithelial cancers. Therefore, a more detailed understanding of the structure and

function of this enzyme is essential. Recently, mutations in UGDH were identified that are associated with congenital heart defects. These mutations cause a change in oligomeric state of the enzyme from a hexamer to a dimer. This shift in oligomeric state may explain the observed phenotype. Therefore, understanding the differences in *in vitro* and *in vivo* activity and regulation between the wild-type hexameric enzyme and the mutant dimeric enzymes is essential to understanding the function of UGDH in development and may provide insight into the role of UGDH in progression of epithelial cancers.

1.4 Glutathione

Like UDP-glucuronate, glutathione is an essential cellular metabolite, not only because of its role in cellular detoxification, but also because of its significant role as a reductive agent in the oxidative stress response and maintenance of cellular redox homeostasis [5, 6, 36]. Glutathione is also important for cysteine storage and transport and in altering sulfhydryl accessibility to modulate signaling pathways and regulate enzyme activity [38, 49, 90].

Glutathione is a tripeptide composed of glutamate, cysteine, and glycine. It is synthesized by the sequential action of two enzymes, glutamate cysteine ligase and glutathione synthetase [76, 97]. In the first and rate-limiting step of glutathione biosynthesis, glutamate cysteine ligase combines cysteine and glycine to form □-glutamylcysteine in an ATP-dependent reaction [37]. Next, glutathione synthetase, also requiring ATP, adds glycine

to form reduced glutathione [37, 38]. Oxidized glutathione is efficiently reduced by glutathione reductase, a flavoprotein that uses NADPH as a reductant, to maintain the cytosolic pool of glutathione in a reduced state [39].

1.5 Glutamate Cysteine Ligase

Glutamate cysteine ligase (GCL) is a cytosolic protein responsible for the first and rate-limiting step of glutathione biosynthesis. In humans and other higher eukaryotes, GCL is composed of heavy catalytic subunit (73 KD) and a light modifier subunit (30 KD) [40, 41]. The catalytic subunit is sufficient for catalysis, while the modifier subunit is known to enhance the activity of the catalytic subunit [44]. Additionally, the availability of the modifier subunit contributes to regulation of enzyme activity by limiting formation of the more active heterodimer. GCL is also regulated by feed-back inhibition by the down-stream product, glutathione [42]. Glutamate cysteine ligase has been widely characterized in a number of organisms. Characterizations of glutamate cysteine ligase have revealed much about both the complex reaction mechanism of the enzyme and the enzyme's *in vivo* functioning and regulation.

Three classes of GCL have been denominated based on sequence conservation: the □ -proteobacteria (group 1), the non-plant eukaryotes (group 2), and the plants and □-proteobacteria (group 3). However, functional characterizations and comparisons of the crystal structures of *E.coli* (Group1)

and *B. juncea* (Group 3) with the recently published *S. cerevisiae* (group 2) structure have indicated that the reaction mechanism between groups is likely to be very similar [43-47]. Although the *S. cerevisiae* enzyme lacks a modifier subunit, it has 45% sequence identity with the human catalytic subunit [45]. Consequently, the *S. cerevisiae* structure has allowed for an accurate model of the human enzyme catalytic subunit to be generated, providing further insights into the catalytic mechanism.

The first step of the catalytic mechanism is an inline attack of the □-phosphate of ATP by the □-carboxylate of glutamate to form a □-glutamylphosphate intermediate [48]. Next, the □-amino group of cysteine performs a nucleophilic attack, releasing the phosphate and forming the product □-glutamylcysteine [49, 50]. The active site is particularly complex due to the presence of three bound magnesium ions and three substrates: glutamate, cysteine, and ATP. While debate exists over whether the substrates are ordered or enter the active site randomly, the examination of the human homology model based on the *S. cerevisiae* structure suggests, at least, that glutamate enters the active site before ATP and cysteine [44].

Glutathione biosynthesis is carefully controlled by regulation of GCL at multiple levels. At the post-translational level, glutathione acts as a feedback inhibitor, while cysteine availability controls the overall rate of the reaction [38, 42]. The association of the modifier subunit with the catalytic subunit has a significant impact on activity; mice without the modifier

subunit produce approximately 10-20% the normal amount of glutathione [51]. Because GCLM availability limits heterodimer formation, increased expression of the modifier subunit may enhance GCL activity [51-54]. Heterodimer formation appears to be regulated by one or more non-essential disulfide bonds between the subunits and possibly by other post-translational modifications or inter-subunit interactions [55, 56].

GCL activity is also increased in response to oxidative stress without production of additional protein [51, 57, 58].

Additionally, glutamate cysteine ligase is subject to extensive transcriptional regulation. The human GCLM and GCLC transcripts are located on different chromosomes and are therefore subject to different regulation [51, 59, 60]. Furthermore, the levels of GCLM and GCLC vary widely in different human tissue types [61]. A number of transcriptional regulatory factors have been identified that interact with GCL promoters. These include Nrf2, AP1, AP3, NFκB, Maf proteins, JunD, Fra, and CREB [62].

Not surprisingly, glutamate cysteine ligase has been associated with numerous diseases. Failure of glutathione production impacts the progression of many diseases, including HIV, cancer, cystic fibrosis, Alzheimer's disease and Parkinson's disease [63]. The importance of GCL to cellular homeostasis and human health is highlighted by the fact that GCLC null mice are embryonic lethal [64]. Interestingly, the absolute requirement for GCLC appears to be satisfied even in the heterozygous state when dramatically

lower levels of glutathione are produced. Recently, GCLC mutations have been identified in individuals with hereditary glutathione deficiency, a disease characterized by hemolytic anemia and sometimes accompanied by neurological degeneration [65-69]. The erythrocyte glutathione levels in individuals homozygous for the mutations were >10% of normal levels. Because none of these mutations lie in the GCLC active site, it is not clear why they cause such a dramatic reduction in glutathione levels. Further studies of the mutations involved in this disease have the potential to lend significant insight into GCLC function. This work details our investigation of these GCLC mutants including assessment of glutathione production in GCLC null mouse embryonic fibroblast cells and the GCLC null *S. cerevisiae* ΔGSH1 strain, as well as, kinetic characterizations in the presence and absence of the modifier subunit.

Chapter 2

Effects of altered oligomeric state on UDP-glucose dehydrogenase function *in vitro* and *in vivo*

Note: The results described in this chapter are being prepared for publication and were completed by Melanie Neely Willis, Katie Easley, Alisha O' Malley, Joseph J. Barycki, Melanie A. Simpson, and members of Jeroen Bakker's laboratory.

2.1 Introduction

UDP-glucose dehydrogenase catalyzes the conversion of UDP-glucose to UDP-glucuronate via two successive oxidations, concomitantly converting two molecules of NAD^+ to NADH. UDP-glucuronate is an essential precursor for protein glycosylation, production of extracellular matrix polysaccharides and is necessary for cellular detoxification of xenobiotics and endobiotics via UDP-glucuronosyltransferases [8, 20]. Availability of UDP-glucuronate and UGDH expression have been implicated in a variety of epithelial cancers and in developmental abnormalities [70-76]. Therefore, a detailed understanding of the structure, function, and regulation of UGDH is essential.

While UDP-glucuronate is implicated in a variety of cellular processes, recent advances in understanding both developmental abnormalities and cancer progression associated with UGDH have highlighted the role of hyaluronan, a key extracellular matrix polysaccharide in causation of both processes [75]. The common link between development and cancer progression is hyaluronan's promotion of cell migration and proliferation. While the types of cancer associated with increased hyaluronan production include breast, head and neck, ventricle, colon, and pancreas cancer [31]; hyaluronan and UGDH have received significant attention in prostate cancer progression, and UGDH has been named as a potential biomarker for prostate cancer [77]. While much has already learned about UGDH, these advances demonstrate the necessity of fully delineating the many factors that control

UGDH function in the cell.

Detailed kinetic characterizations and mutation of key catalytic residues by our lab and other groups have illuminated key steps in the reaction mechanism of UGDH. These studies have been greatly aided by modeling the human enzyme using the available *S. pyogenes* crystal structure (PDB ID: 1DLJ) and later, the *C. elegans* (PDB ID: 2O3J) and human crystal structures (PDB ID: 2QE3). Early studies of the UGDH catalytic mechanism were made using *S. pyogenes* and bovine liver enzyme. A Bi-Uni-Uni-Bi Ping Pong mechanism was proposed in which the mechanism proceeded through an UDP-aldehyde intermediate that was trapped by an active site lysine to form a Schiff base intermediate [19, 78, 79]. An active site cysteine would then attack the Schiff base, and the reaction would proceed to completion through a thiohemiacetal intermediate, followed by further oxidation to a thioester intermediate and hydrolysis to yield the product. Ultimately, the formation of a Schiff base has been discredited [20, 23]. Kinetic data from our lab suggest that in the human enzyme, K270 serves to position D280 in the active site, which, in turn positions and activates a catalytic water molecule. The water molecule may then directly abstract a proton from the 6′ hydroxyl of UDP-glucose in the first oxidation step and be repolarized by K220. The repolarized water might then activate the catalytic cysteine, C276, allowing attack to form the thiohemiacetal intermediate. The K220 residue could then serve to stabilize the oxyanion charge during formation of the thioester intermediate and hydrolysis to yield the product, UDP-glucuronate [20, 22].

In recent years, the knowledge of UDP-glucose dehydrogenase regulation *in vivo* has rapidly advanced fueled, in part, by the association of UGDH with various cancers and developmental aberrations. Several studies have reported that the UGDH gene is under the control of the peroxisome proliferative receptor α (PPAR α) response element, allowing an up-regulation of UGDH in response to some xenobiotics [27, 28]. Similarly, UGDH has been demonstrated to be up-regulated at the transcriptional level in response to androgens in certain cancers [24-26]. These findings are not surprising considering the key role UGDH plays in detoxification and epithelial cancer progression, and future studies will likely expand and confirm the role of transcriptional regulation in UGDH function and malfunction.

UGDH is also subject to extensive post-translational regulation, including inhibition by UDP-xylose, quercetin, and gallic acid [9, 20, 21]. UDP-xylose is produced from UDP-glucuronate in the ER and Golgi lumen, making it a potent feedback inhibitor [Bakker]. Quercetin and gallic acid are both members of the class of compounds known as polyphenols that have recently been linked with prostate cancer tumor suppression [21]. While quercetin and UDP-xylose have been proposed to be competitive inhibitors of UDP-glucose in the enzyme active site, gallic acid was found to be a non-competitive inhibitor [9, 21]. Additionally, UDP-xylose was shown to have effects on allosterism, and quercetin was found to have mixed-type inhibition with respect to NAD^+ [20, 21]. A large-scale screen of chemicals by our lab revealed a number of novel inhibitors that have yet to be characterized.

Thus, it is possible that post-translational regulation of UGDH may proceed by binding or interaction with sites on the surface of the protein, distant from the enzyme active site. This possibility is significant because bacterial forms of UGDH are dimeric, while human and other higher species have a hexameric structure, a trimer of active dimers (Figure 2.1). In the human enzyme, regulation may occur at sites not found in the dimeric enzyme, such as at the dimer-dimer interface.

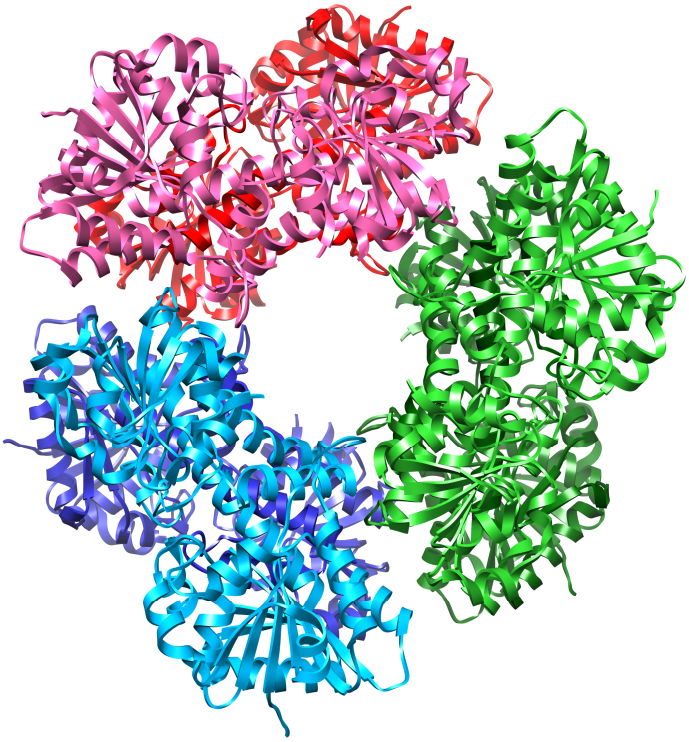

Figure 2.1. The human UDP-glucose dehydrogenase is a homohexamer. In humans and other vertebrates, UGDH exists as a hexamer, a trimer of catalytically active dimers. Here one dimer pair is shown in pink/red, one in blue/cyan and one in dark green/light green. PDB ID: 2Q2E.

Furthermore, recent studies by our collaborator, Jeroen Bakker, have revealed that certain mutations in human UGDH are associated with congenital heart defects [80]. Further studies of these two mutants, UGDH

E416D and UGDH R141C, confirmed the link between these mutations and aberrant cardiac development in zebra fish. Knockdown of UGDH using a morpholino in zebra fish embryos caused a dramatic increase in cardiac edema. Yet, this phenotype was almost wholly abolished by addition of wild-type UGDH RNA. Partial rescue was observed when either UGDH E416D or UGDH R141C RNA was added (Figure 2.2), indicating that there are *in vivo* differences in the functioning of these two mutant UGDHs compared to wild-type.

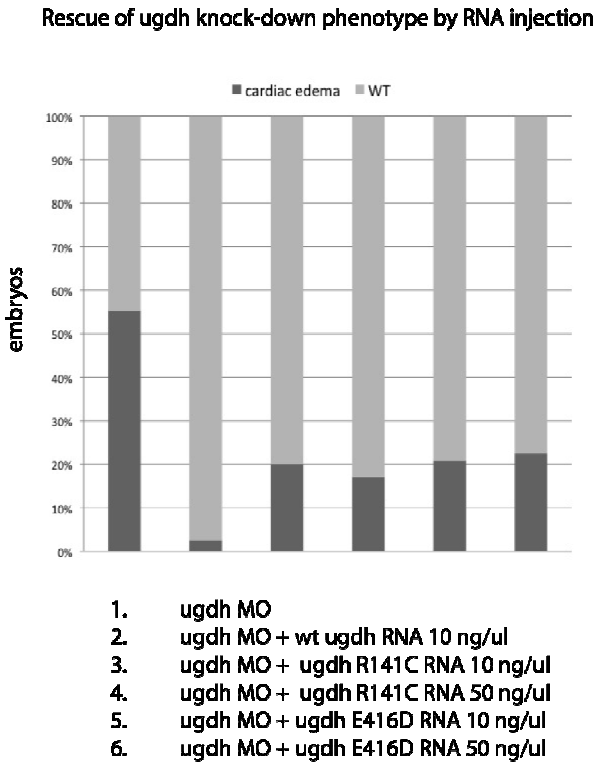

Figure 2.1. Rescue of UGDH knockdown phenotype by RNA injection. Shown in the above figure is the percentage of embryos developing an aberrant phenotype of cardiac edema (dark grey bar) versus a wild-type phenotype (light grey bar) for each population. The different populations are enumerated and correspond to each bar from left to right and indicate the type of treatment. All embryos contain an UGDH morpholino to knockdown UGDH expression. Selected populations were injected with human wild-type or UGDH E416D or UGDH R141C RNA with a concentration of either 10 ng/μl or 50 ng/μl.

Although these two mutations have a demonstrated phenotype in zebra fish embryos, examination of the human crystal structure of UGDH reveals that these two mutations are neither located in, nor are very close to the enzyme active site. This observation raises the intriguing possibility that rather than directly altering enzyme catalysis, these mutations may be important to enzymatic regulation.

In conclusion, understanding the function of human UGDH has become more urgent as UGDH has been associated with an ever-increasing number of epithelial cancers and developmental defects. Initial characterizations of the two UGDH clinical mutants have revealed *in vivo* differences in zebra fish that are similar to a human phenotype associated with these mutations. Based on the location of these two mutations distant from the enzyme active site, these mutants may alter *in vivo* regulation rather than directly alter catalysis. Determination of the *in vivo* effects of these mutants on UGDH activity is essential to understanding the development of adverse phenotypes and disease progression by providing insight into enzyme regulation and activity.

2.2 Materials & Methods

Generation of Mutant UGDH plasmids & Protein Expression and Purification

For expression in HEK 293 cells, the clinical and engineered dimer point mutants of UGDH were generated from the wild-type UGDH-pIRES construct using the Quik Change site-directed mutagenesis kit according to

manufacture instructions (Stratagene). Sequences were verified by Eurofins MWG Operon.

The human enzyme (PDB ID: 2Q2E) was examined in Chimera and residues participating in hydrogen bonding at the dimer-dimer interface were identified. Suitable candidates were chosen for mutagenesis directed at disrupting the dimer-dimer interface and destabilizing hexamer structure. The wild-type UGDH-pET28a construct was subjected to mutagenesis using the Quik Change site-directed mutagenesis kit (Stratagene). Sequences were verified by the University of Nebraska Genomics Core.

Proteins were expressed and purified as previously described [22]. Briefly, the N-terminal his-tagged plasmids for wild-type UGDH and each mutant were transformed in Rosetta2 (DE3)pLysS *E. coli* cells (Novagen). The next day, cells were grown in 2xTY media with 30 mg/L kanamycin at 37°C until reaching an A_{600} of 0.6. The temperature was then reduced to 30°C, and protein expression was induced by addition of a final concentration of 0.5mM IPTG. After an hour, the temperature was reduced to 18°C, and the cells were grown overnight. The next day, the cells were harvested by centrifugation.

The harvested cells were resuspended in 50mM sodium phosphate buffer, 0.3M sodium chloride, 10mM imidazole, pH8 with 1mg/ml lysozyme. The solution was then sonicated to ensure lysis. After centrifugation to remove cellular debris, the supernatant was loaded onto a 5ml Ni-NTA His•Bind column (Novagen) and purified according to the manufacturer's

instructions. The eluted protein was then dialyzed overnight at 4°C against 0.1M sodium phosphate, pH 7.4, flash frozen in liquid nitrogen, and stored at -80°C.

Gel Filtration

The molecular weight of each mutant and wild-type UGDH was determined by gel filtration chromatography to determine the oligomeric state of each enzyme. Each enzyme was dialyzed in 0.15M sodium chloride, 50mM tris, 1mM DTT, pH 7.4 and loaded onto a Superdex 200 HR 10/30 column (GE Healthcare Lifesciences). The FPLC flow rate was 1 ml/min, and a protein standard run was also performed using the following proteins: thyroglobin (669 KD), ferritin (440 KD), aldolase (158 KD), ovalbumin (43 KD), ribosome protein A (13.7 KD). The peaks for each wild-type and mutant UGDH were compared to the standard proteins to determine the approximate molecular weight and the corresponding oligomeric state of each species.

Analytic Ultra-centrifugation Sedimentation Velocity Experiments

Sedimentation velocity experiments were performed to confirm the oligomeric state of the engineered dimer mutants. Purified wild-type, T325A and E110A UGDH protein was dialyzed against 0.15M sodium chloride, 50 mM sodium phosphate buffer and diluted to 1 mg/ml. The mutant and wild-type enzymes were loaded into analytic cells and were centrifuged at 42,000 rpm for 18 hours in a Beckman Coulter ProteomeLab XL-1 centrifuge. A preliminary examination of the data showed that the 1 mg/ml concentration

was ideal, so further analysis was performed using this data. The data was analyzed using SedFit [81] to find the molecular weights of the protein complexes.

Kinetic Characterizations

The *in vitro* activity of each wild-type and mutant UGDH was characterized using a standard kinetic assay as previously described [22]. For each of the two substrates, NAD^+ and UDP-glucose, the concentration of one substrate was held constant at a saturating concentration, while the other was varied from 1- 10mM to determine the kinetic constants, K_m and V_{max}. All reactions were performed in a cuvette containing 500 μl of the substrates in 50mM sodium phosphate buffer. The reaction was initiated by the addition of 0.01mg of protein and monitored at 340nm for 1 minute to measure the generation of NADH. The saturating concentration of NAD^+ was 2mM, and the saturating concentration of UDP-glucose was 200μM. All reactions were performed in triplicate, and the change in absorbance over time was recorded. The values were analyzed using Prism Graphpad software. The change in absorbance was converted to mg/ml/min by multiplying the reaction volume and dividing by the amount of protein and the extinction coefficient of NADH. These values were plotted against concentration and fitted to a Michaelis-Menten curve. The apparent V_{max} and K_m were determined from these curves for each of the substrates.

To determine the loss of activity over time of engineered dimer mutants, aliquots of 1mg/ml UGDH T325A, UGDH E110A and wild-type UGDH were placed at 37°C and periodically the activity of each was measured using the standard kinetic assay described above. A saturating concentration of UDP-glucose and NAD^+ was used. The stability of the clinical dimer mutants, UGDH E416D and UGDH R141C, was determined in a similar manner except that 1:1 mixtures of each mutant with wild-type were also evaluated.

Transient Transfections

To measure the concentration of UDP-glucuronate *in vivo* in response to each mutant and wild-type UGDH protein, HEK293 cells were transiently transfected to over-express each of the four dimeric mutants, wild-type, and the blank GFP vector. Untransfected cells were also treated similarly and used as a control. The HEK 293 cell line was chosen, both for the ease of transfection and because previous work has demonstrated it contains comparably low levels of UGDH enzyme. The cells were collected and metabolite levels and protein expression were measured. In addition, another set of transfections included wild-type UGDH, controls cells, the GFP vector and a catalytically dead UGDH mutant previously characterized by members of our lab, UGDH D280N.

HEK293 cells were cultured in DMEM 1X media with 10% fetal bovine serum in 10 cm plates at 37°C and 5% carbon dioxide and transiently

transfected using the calcium phosphate method with wild-type and mutant UDP-glucose dehydrogenase in a GFP pIRES vector. The day before transfection, the cells were split to 30% confluency. The day of the transfection, the serum-containing media was removed and the cells were washed twice with serum-free DMEM 1X. To transfect the cells, 1 X TBS was added to the plasmid DNA and incubated for 5 minutes. 2.5 M calcium phosphate was then added, and the mixture was incubated for 7 minutes. The mixture was then added drop-wise to the cells. The cells were incubated overnight and the media was removed and replaced with DMEM 1X + 10 % fetal bovine serum.

The cells were harvested the next day by lifting with trypsin. The cells were washed twice with cold PBS 1X. A quarter of the resuspended cells were set aside for Western blotting and a sample was taken to count the cells for each construct. The remaining cells were set aside for metabolite measurements using HPLC. All cell samples were flash frozen in liquid nitrogen and stored at -80°C.

Verification of Protein Expression by Western Blot

Western blotting was performed to verify and quantify expression of UGDH for each transfected construct. Briefly, cells were lysed in RIPA buffer with protease inhibitors, incubated on ice, and centrifuged to remove cellular debris. A Bradford protein assay was performed to determine the protein concentration of each sample [82]. The samples were then combined with

loading buffer, heat denatured, and run on a 12% SDS-Page gel. The proteins were transferred to a polyvinylidene fluoride membrane. The membrane was simultaneously probed with anti-UGDH and anti-β-tubulin antibodies. An Odyssey Infrared Imaging System (LI-COR) was used to detect fluorescent secondary antibodies: Alexa Fluor 688 anti-mouse IgG (Invitrogen; β-tubulin) and IRDye 800 anti-rabbit IgG (Rockland; UGDH). The intensity of each band was measured and used in further analysis.

Measurement of UDP-glucuronate & related metabolites by HPLC

A method to prepare samples and perform HPLC was developed based on previous methods [83, 84]. To perform HPLC quantification cells were lysed by addition of 0.75M perchloric acid and proteins were removed by centrifugation. The lysates were neutralized using 5M potassium hydroxide, taking care not to raise the pH above ~6. Then, the lysates were centrifuged to remove the salt. The sample was immediately loaded onto the HPLC column.

The HPLC experiments were performed using a Waters spherisorb SAX (strong anion exchanger) 5.0 μm, 4.6 mm x 150 mm column attached to a Beckman System Gold Solvent Module and Detector 166 machine. Mili-Q filtered water and 3.5 M ammonium phosphate were used as the mobile phase. All buffers were filtered using a 0.22 μm filter (Whatman, Gmb.). Each HPLC run consisted of a 5 minute water wash followed by a linear gradient of ammonium phosphate from 0 to 100% over 30 minutes. The run was

concluded by flushing with 100% ammonium phosphate before returning to 100% water over 5 minutes and then flushing with water for 10 minutes. Peak data was recorded at 254 nm and 1 Mhz. Each set of transfectants was run sequentially after first running a blank wash run and a run containing a mixture of nucleotide standards. The nucleotide standard mix included the following: 1mM NAD^+, 1mM NADH, 1mM ATP, 1mM CTP, 1mMUTP, 1mM GTP, 0.5M UDP-glucose, 0.5mM UDP-galactose, 0.5mM uridine monophosphate, and 1mM UDP-glucuronate.

The data were analyzed as follows. Peaks were assigned to the standard mixture by running each standard separately to determine retention time and peak shape. The standard mixture of each data set was then used to assign peaks to each sample run. A peak area report was generated using the 32 Karat Software, v. 5.0 (Beckman Coulter), and the area of each peak was considered to be the raw metabolite measurement. These raw numbers were normalized to total protein levels as determined by the Bradford assay. These numbers were then entered into Prism Graphpad software to generate bar charts to compare the relative concentration of each identified metabolite in each of the transfectants.

2.3 Results

Protein Expression & Gel Filtration of the Clinical UGDH mutants

The mutant UGDH constructs were successfully generated from our wild-type pET 28 construct. Each mutant UGDH was expressed and purified

as soluble protein. Gel filtration chromatography, a typical final step in protein purification protocols, yielded surprising information about UGDH E416D and UGDH R141C. While the wild-type protein has previously been observed by members of our lab to elute almost exclusively as a single peak of ~360 KD, both of the clinical mutants were found to have altered oligomeric state compared to wild-type (Figure 2.3). UGDH E416D was found as a single peak of ~120 KD, while UGDH R141C eluted as two nearly equal peaks, one at ~120 KD and one at ~360 KD. Since each UGDH monomer has a molecular weight of ~60 KD, a dimer would be expected to have a weight of ~120 KD and a hexamer of ~360 KD. A standard curve of elution times versus the standard protein molecular weight was created, and the equation of the line was solved for the wild-type and mutant UGDH protein weights. This confirmed that wild-type UGDH is a hexamer, UGDH E416D is a dimer, and UGDH R141C exists in equilibrium between dimer and hexamer.

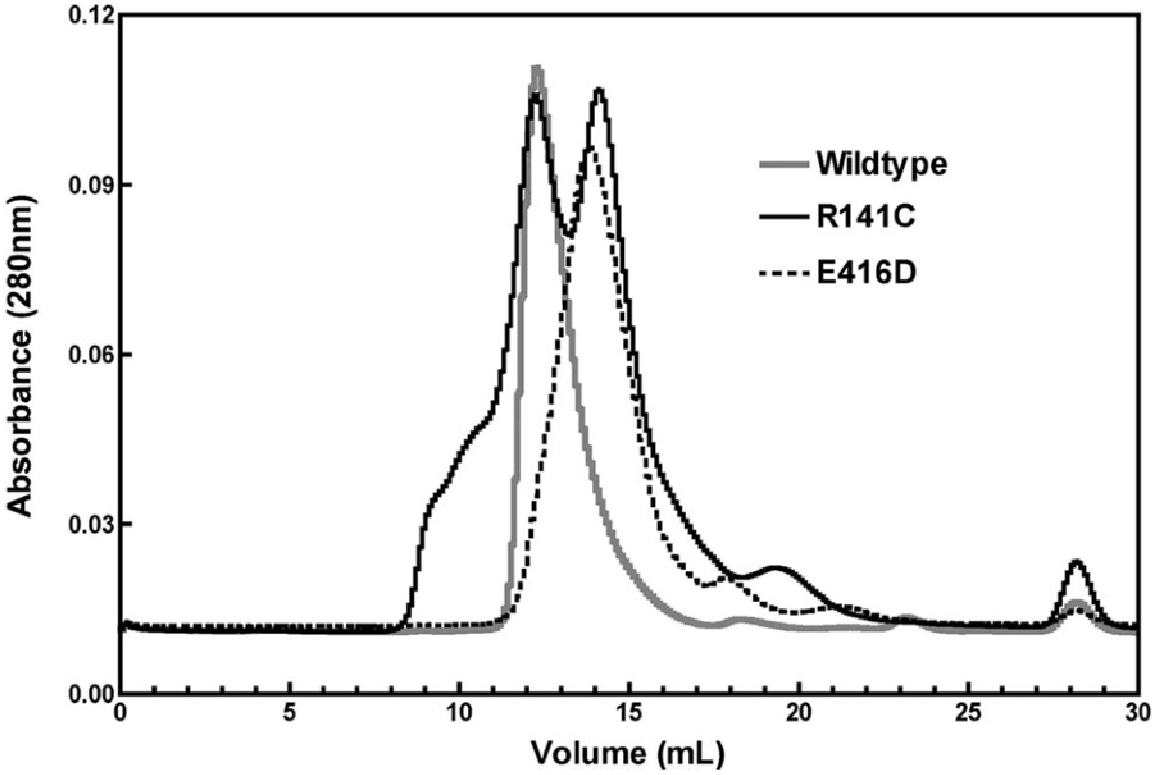

Figure 2.2. Gel filtration of the clinical UGDH mutants. Shown are UGDH E416D (dashed black), UGDH R141C (black), and wild-type UGDH (grey) size-exclusion chromatography gel filtration traces. Wild-type UGDH and UGDH E416D each elute as a single peak representing the hexameric and dimeric species, respectively. UGDH R141C elutes as two peaks, demonstrating the presence of both the dimeric and the hexameric species.

Kinetic characterization of the clinical UGDH Mutants

These mutants, UGDH E416D and UGDH R141C, were further characterized to reveal that their *in vitro* activity is nearly equivalent to wild-type activity, though R141C exhibits slightly diminished activity and tighter binding of both substrates (Table 2.1). Bacterial species are known to have dimeric UGDH, and it has been hypothesized that each of the dimers composing the wild-type hexamer UGDH contained a functional active site. Thus, it might be expected that a human dimer has similar activity to human hexamer. Our results revealed that the clinical mutants have comparable *in*

vitro activity compared the wild-type enzyme.

Table 2.1. Apparent kinetic constants for the clinical UGDH mutants.

Protein	**UDP-Glucose**		**NAD^+**	
	V_{max} μmol/min/mg	**K_m** μM	**V_{max}** μmol/min/mg	**K_m** μM
Wild-type	1.011 ± 0.0297	27.01± 2.459	1.140 ± 0.0235	576.5± 29.26
E416D	1.017 ± 0.0268	33.23 ± 2.908	1.217 ± 0.0403	576.7 ± 46.99
R141C	0.547 ± 0.0093	16.04 ± 1.253	0.534 ± 0.011	375.1 ± 23.93

In vitro Stability Assays

Furthermore, *in vitro* assays were performed to determine the loss of activity of each of the mutants at 37°C over time, with both mutant-only samples and mutant mixed with wild-type samples to recapitulate the heterozygous state (Figure 2.4).

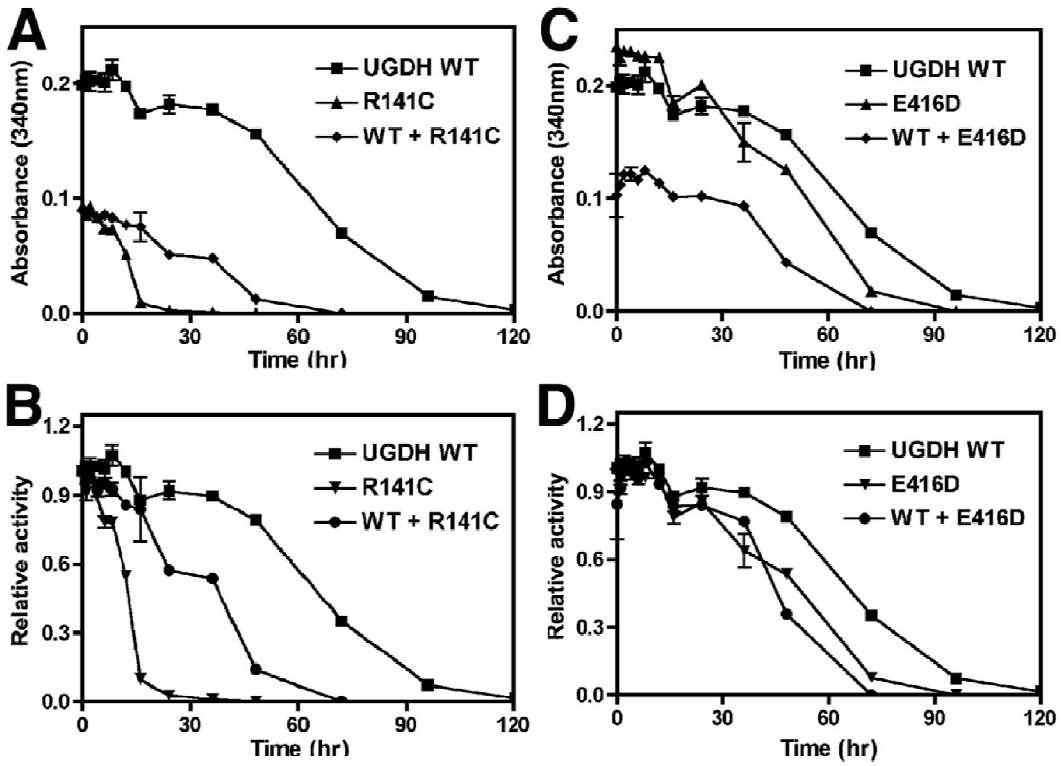

Figure 2.3. Loss of UGDH activity over time at 37°C. Panel A displays the loss of activity over time of UGDH R141C (triangle), a 1:1 mixture of wild-type and UGDH R141C (diamond), and wild-type (square) as a function of activity measured by the standard kinetic assay following NADH generation at 340 nm. **Panel B** represents this data as a loss in activity of each enzyme or mixture where the initial activity is set equal to one for wild-type (square), UGDH R141C (triangle), and UGDH R141C + wild-type (circle). **Panel C** displays the loss of activity over time of UGDH E416D (triangle), a 1:1 mixture of wild-type and UGDH E416D (diamond), and wild-type (square) as a function of activity measured by the standard kinetic assay following NADH generation at 340 nm. **Panel D** represents this data as a loss in activity of each enzyme or mixture where the initial activity is set equal to one for wild-type (square), UGDH E416D (triangle), and UGDH E416D + wild-type (circle).

These studies indicate that UGDH E416D alone has a half-life similar to wild-type UGDH. UGDH R141C, the mutant having mixed dimeric and oligomeric state has a dramatically reduced half-life compared to wild-type UGDH, which was slightly improved when mixed with wild-type UGDH. However, the mixture of the dimeric UGDH E416D with wild-type UGDH displays a reduced half-life compared to both UGDH E416D and wild-type

UGDH alone. This result indicates that the mutant UGDH dimer may disturb the ability of the wild-type dimers to trimerize into normal wild-type hexamers. Thus, the clinical UGDH mutants may interfere with normal protein stability and also may perturb allosteric regulation mechanisms *in vivo* due to either dimeric character or to some other undiscovered property of these two mutant proteins.

Creation of the Engineered UGDH Dimer Mutants

In order to distinguish between these two possibilities, we deemed it prudent to create additional mutant UGDH enzymes existing wholly in the dimeric state to clarify the effects of dimeric state on *in vitro* and *in vivo* UGDH function. To do this, we examined the dimer-dimer interface of the human UGDH crystal structure (PDB ID: 2Q2E)(Figure 2.5).

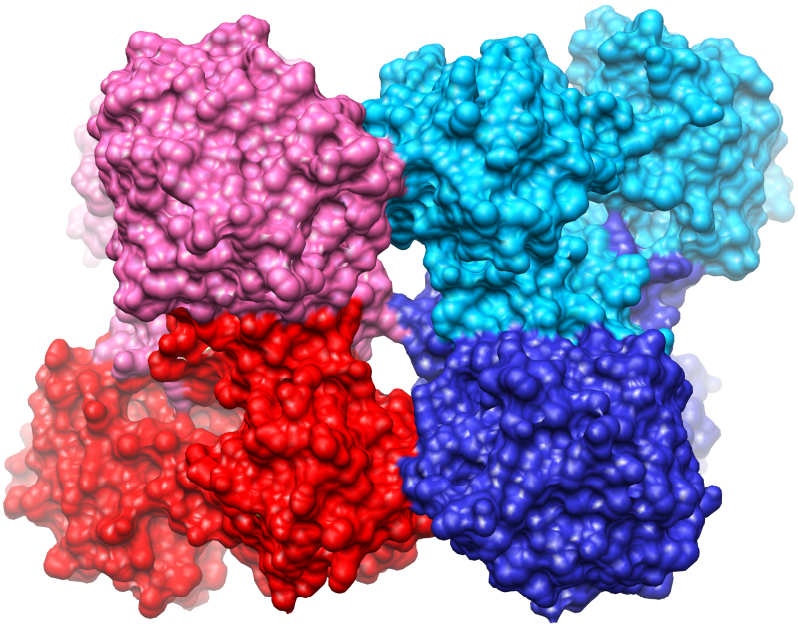

Figure 2.4. The dimer-dimer interface of UDP-glucose dehydrogenase. Shown here is the human hexamer turned on its side to view the dimer-dimer interface of the pink/red dimer and the cyan/blue dimer. The light green/dark green dimer would be directly behind the shown dimer-dimer pair.

Hydrogen bonds between adjacent dimers were identified and single mutations were made in hopes of disrupting the dimer-dimer interface. E110 was identified as a residue that hydrogen bonds with K329 on the adjacent dimer. Additionally, E110 forms an inter-helical hydrogen bond with R114. Thus, mutating E110 has the potential to not only disrupt the dimer-dimer interface, but also, to compromise the structural stability of each monomer. On the other hand, T325 does not directly bond with the adjacent dimer. Instead, it participates in a network of hydrogen bonds between the two dimers. T325 forms a hydrogen bond with K339, which forms a hydrogen

bond with E110 in the adjacent dimer. Therefore, it is likely that mutating T325 will disrupt the hydrogen bond between K339 and E110, though the inter-helical bond between E110 AND R114 should remain intact. Both of these residues, E110 and T325 were mutated to alanine, in order to neutralize the charge-based interactions and not cause any unintended structural perturbations. UGDH T325A and UGDH E110A were generated and successfully purified as soluble proteins. Similar to the clinical mutants, these mutations were distant from the enzyme active site (Figure 2.6).

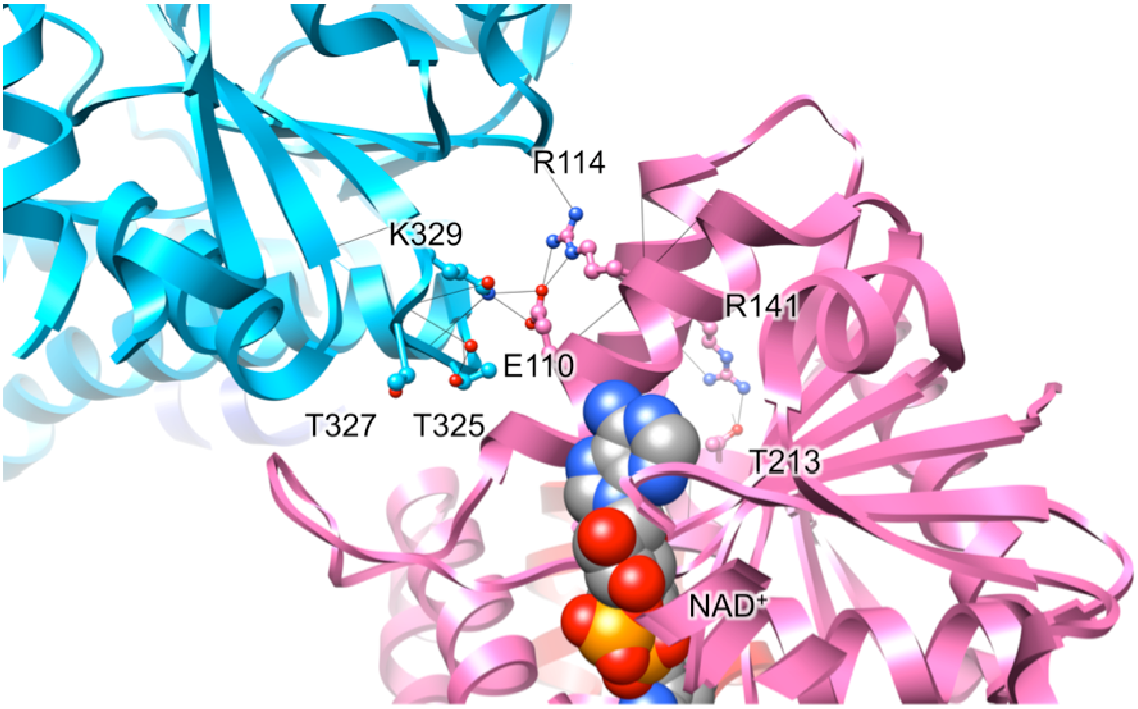

Figure 2.5. Location of the Engineered Dimer Point Mutant Residues. Shown here is a close-up of part of the dimer-dimer interface of UGDH. NAD^+ is shown in a space-filling model in the lower right side of the image. Residues participating in hydrogen bonds disrupted by the mutations are shown, and hydrogen bonds are shown as black lines.

Gel filtration of the Engineered Dimer Mutants

After protein expression and purification, we performed gel filtration to determine whether the mutants eluted as hexamers, dimers, or in an equilibrium between the two. Gel filtration confirmed the expected hexameric state of wild-type UGDH and revealed that both the mutants, UGDH E110A and UGDH T325A, were dimers rather than hexamers. Since each UGDH monomer has a molecular weight of ~60 KD, a dimer would be expected have a weight of ~120 KD and a hexamer of ~360 KD. The wild-type protein eluted between the aldolase (158 KD) and the ferritin (440 KD) proteins, consistent with a molecular weight of ~360 KD. In contrast, both the mutants eluted between ovalbumin (43 KD) and aldolase (158 KD), consistent with a molecular weight of ~120 KD (Figure 2.7).

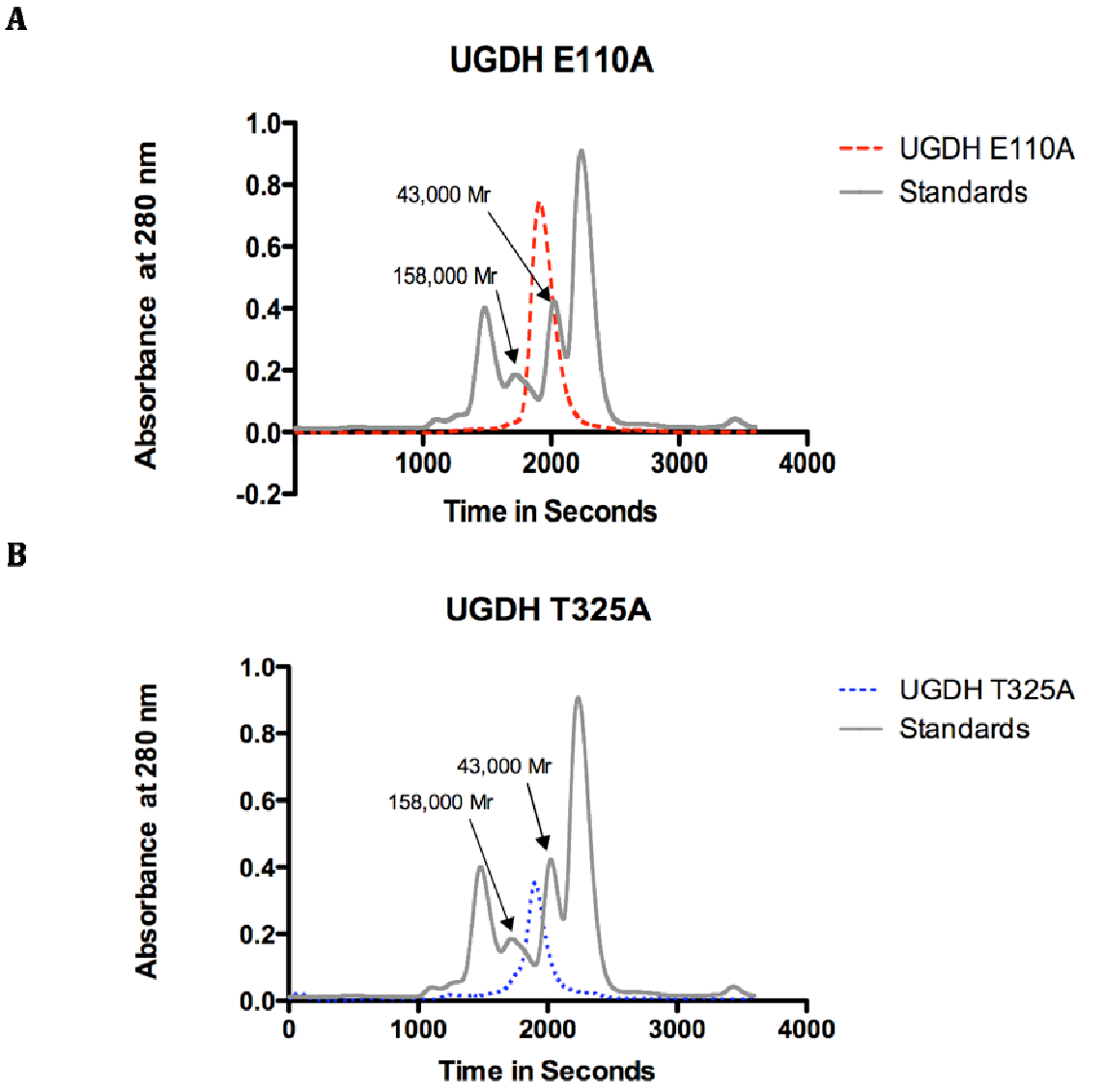

Figure 2.6. panel A. Gel filtration of UGDH E110A. Shown are UGDH E110A (dashed red) and the standard proteins (grey) size-exclusion chromatography gel filtration traces. The standard proteins included thyroglobin (669 KD), ferritin (440 KD), aldolase (158 KD), ovalbumin (43 KD), and ribosome protein A (13.7 KD). UGDH E110A eluted between ovalbumin and aldolase, indicating a dimeric state. **Panel B. Gel filtration of UGDH T325A.** Shown are UGDH T325A (dashed blue) and the standard proteins (grey) size-exclusion chromatography gel filtration traces. The standard proteins included thyroglobin (669 KD), ferritin (440 KD), aldolase (158 KD), ovalbumin (43 KD), and ribosome protein A (13.7 KD). UGDH T325A eluted between ovalbumin and aldolase, indicating a dimeric state.

Analytic Ultra-centrifugation Sedimentation Velocity Experiments

Analytic ultra-centrifugation sedimentation velocity experiments also confirmed that the oligomeric state of each of the engineered mutants was dimeric. Sedimentation velocity experiments have the advantage of both determining the number of species present in a mixture and determining a very accurate molecular weight for each species. Interestingly, the sedimentation velocity experiments demonstrated that the oligomeric state for wild-type was not wholly hexameric; a very small amount of the wild-type protein existed as a dimer. Similarly, the mutant UGDH T325A showed a very small amount of protein in the hexameric state. In both cases, the amount of protein in the minor species could be approximated at less than 5% of the total. In contrast, the mutant UGDH E110A existed as a dimer, without a hexameric peak.

Table 2.2. Molecular Weights Determined by Sedimentation Velocity

Protein	**Molecular Weight (KD)**
Wild-type	352
E110A	137
T325A	122

The molecular weights of the two dimer mutants varied slightly. UGDH E110A had a molecular weight of 137 KD, while T325A had a molecular weight of 122 KD. The minor peak of wild-type UGDH had a molecular weight of 132 KD, corresponding to a small amount of dimer protein. The major peak of wild-type UGDH was at 352 KD, while the minor peak of UDGH T325A was

at 369 KD. These minor differences in weight between proteins having the same amount of mass reflect the sensitivity of this technique to not only mass, but also, to the shape of each protein as it travels across the solvent during centrifugation. Thus, analytical ultra-centrifugation demonstrated that the mutants UGDH E110A and UGDH T325A were dimers in contrast to the wild-type, hexameric protein.

Kinetic Characterizations of the Engineered Dimer Mutants

After confirming that the engineered mutant UGDH proteins were, indeed, dimers, we characterized them kinetically to determine if there were significant differences between the *in vitro* activity of hexameric and dimeric UGDH proteins. The kinetic data are summarized below (Table 2.3).

Table 2.3. Apparent Kinetic Constants for the Engineered Dimer Mutants

Protein	**UDP-Glucose**		**NAD^+**	
	V_{max} μmol/min/mg	**K_m** μM	**V_{max}** μmol/min/mg	**K_m** μM
Wild-type	.298 $\pm$ .006	7.16 $\pm$ .589	.320 $\pm$ .008	354 $\pm$ 30.8
E110A	.164 $\pm$ .016	21.50 $\pm$ 6.47	.167 $\pm$ .010	186 $\pm$ 58.3
T325A	.337 $\pm$ .009	9.32 $\pm$ .943	.322 $\pm$ .010	331 $\pm$ 38.0

The apparent V_{max} values for the NAD^+ measurement of wild-type and UGDH T325A were in overlapping ranges, and the values for the UDP-glucose

measurement were nearly that close. The apparent K_m values for wild-type UGDH and UGDH T325A were also very similar—the value for UDP-glucose K_m for UGDH T325A was ~28% greater than the value for wild-type UGDH, and the values for NAD^+ were in overlapping ranges.

However, UGDH E110A evidenced slight, but noticeable differences in kinetic constants. The values for apparent V_{max} for UGDH E110A were approximately half those of wild-type UGDH for both the NAD^+ and the UDP-glucose measurements. Additionally, the apparent K_m values were perturbed. For the NAD^+ measurement, the apparent K_m of UGDH E110A was approximately half of the wild-type UGDH value; while for the UDP-glucose measurement, the apparent K_m of UGDH E110A was approximately 3 times the wild-type UGDH value. From the perspective of enzyme kinetics, these values are still similar enough to indicate a highly similar level of activity between both of the dimer mutants and wild-type UGDH. However, the E110A mutant exhibits some noticeable, if slight differences from wild-type UGDH and also has much larger error bars than the other two enzymes, indicating that activity was less consistent between measurements. Therefore, the kinetic characterizations reveal that the engineered dimer mutants have almost equivalent activity to wild-type UGDH, though UGDH E110A exhibits slightly different kinetic constants than the other enzymes.

In vitro Stability Assays

We measured the activity of the engineered dimer mutants and wild-type UGDH after incubation at 37°C to determine if there were differences in protein stability and activity at body temperature (Figure 2.8). Initially, wild-type and UGDH T325A activity were similar, and UGDH E110A activity was approximately half that of wild-type, consistent with the detailed kinetic characterizations. Interestingly, UGDH E110A activity dropped off almost immediately, and after 6 hours, both mutants had dramatically reduced activity compared to wild-type. By 10 hours, all three enzymes had severely impaired activity. After 24 hours, the enzymes were inactive. These data highlight the relative instability of the dimeric UGDH mutants compared to wild-type UGDH, a difference that may have significant effects on *in vivo* enzyme function.

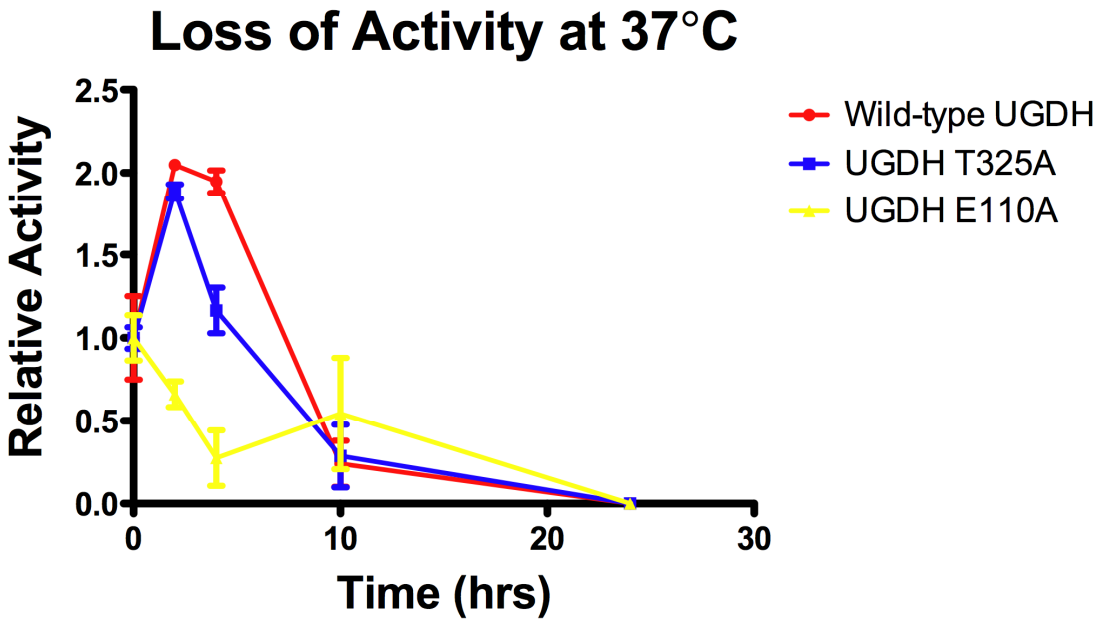

Figure 2.7. Loss of Activity at 37°C. UGDH E110A, UGDH T325A and wild-type UGDH were incubated at 37°C for 24 hours. Periodically, each protein was tested for activity using the standard UGDH activity assay with NAD^+ and UDP-glucose at saturating levels. Assays were performed in triplicate.

Measurement of UDP-glucuronate & related metabolites by HPLC

HPLC metabolite analysis was performed to determine differences in the *in vivo* functioning of the hexameric wild-type UGDH and the clinical and engineered dimeric mutants. This method allowed measurement of both UDP-glucose and UDP-glucuronate. Other related metabolites were also measured including the nucleotide triphosphates, various UDP-sugars, NAD^+, NADH and uridine monophosphate, a breakdown product of UDP.

Initially, Western blot analysis revealed that the untransfected HEK293 cells and the vector-only GFP cells had very small amounts of UGDH,

compared to the wild-type and mutant UGDH transfectants (Figure 2.9). No notable differences in transfection efficiency or UGDH protein expression between wild-type and the dimeric mutants were observed. However, because our results indicate that *in vivo* protein stability may be compromised in the dimeric UGDH mutants, the measured amount of UDP-glucuronate was normalized to total protein levels, as determined by Bradford assay, rather than to UGDH levels.

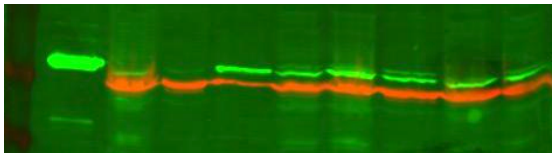

Figure 2.9. UGDH expression in transfected HEK293 cells. Shown here is a representative Western blot to determine UGDH expression in transfected HEK293 cells. The first lane contains the molecular weight marker. The second lane is purified, recombinant UGDH. A green band, showing the anti-UGDH probe, appears at approximately 60KD, the expected molecular weight of UGDH. The red bands show the anti-β-tubulin probe, used as a loading control. The remaining lanes contain in ascending order: untransfected HEK293 cells, vector-only GFP cells, UGDH D280N, wild-type UGDH, UGDH E110A, UGDH T325A, UGDH E416D and UGDH R141C.

Surprisingly, none of the dimeric UGDH mutants showed any significant differences in UDP-glucuronate levels compared to wild-type. While significant differences in UDP-glucuronate levels were not found, we did observe a slight increase in the amount of UDP-glucuronate in wild-type UGDH compared to the mutants (Figure 2.10). Still, these differences were slight and accompanied by large error bars, making any conclusions about *in vivo* UGDH function based on UDP-glucuronate levels problematic. Therefore,

the HPLC measurements of UDP-glucuronate levels did not demonstrate significant differences between the dimeric mutants and wild-type UGDH. Thus, measuring UDP-glucuronate levels as a measure of *in vivo* UGDH enzyme function appears to have limited value. Examination of the levels of UDP-glucose, NAD^+, and NADH were similarly uninformative.

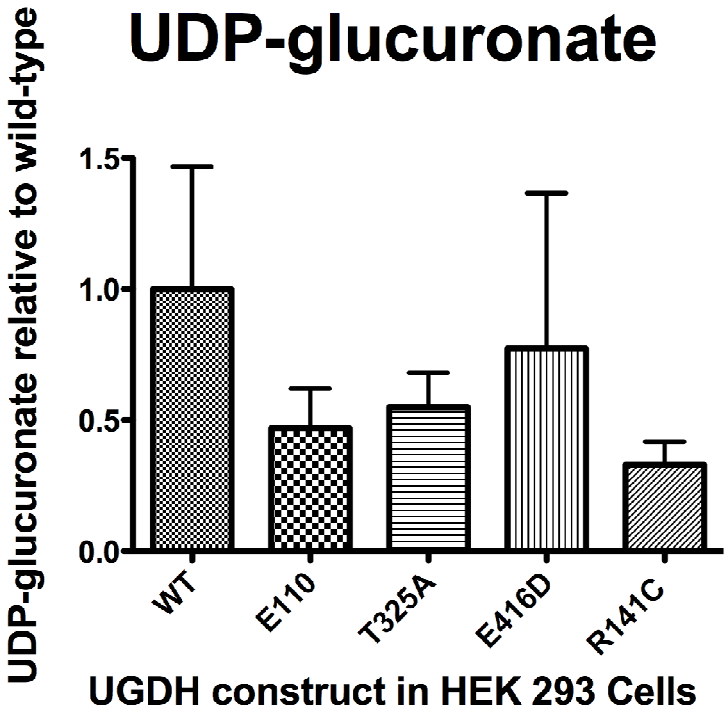

Figure 2.10. Levels of UDP-glucuronate in transfected HEK 293 cells. HEK 293 cells were transiently transfected with each construct. UDP-glucuronate levels were measured by HPLC and normalized to total protein levels. Wild-type level is set equal to one for ease of comparison. Error bars represent the SEM of three replicates. Control and GFP values have been omitted.

2.4 Discussion

The recent identification of two mutations in UDP-glucose dehydrogenase that are associated with human congenital heart defects and an altered oligomeric state bring to light a little-contemplated aspect of *in vivo* regulation that may have dramatic phenotypic consequences. UDP-glucose dehydrogenase catalyzes the conversion of UDP-glucose to UDP-glucuronate via two successive oxidations. UDP-glucuronate is an essential precursor for protein glycosylation, production of extracellular matrix polysaccharides and is necessary for cellular detoxification of xenobiotics and endobiotics via UDP-glucuronosyltransferases [8, 20]. Availability of UDP-glucuronate and UGDH expression have been implicated in a variety of epithelial cancers and in developmental abnormalities [70-76].

The recently identified human UGDH mutants, UGDH E416D and UGDH R141C, were found to exist wholly or partially as dimers, although this change in oligomeric structure was found to not significantly impact *in vitro* catalysis. In order to separate the effects of oligomeric state from other impacts of these individual mutations, we endeavored to engineer and characterize additional dimeric UGDH mutants. This work details our efforts to detect *in vivo* differences in UGDH regulation due to oligomeric state by measuring levels of UDP-glucuronate and other key metabolites in human cells transfected with wild-type UGDH and the mutant UGDHs.

Initial Characterization of the Clinical UGDH Mutants

The UDP-glucose dehydrogenase congenital heart defect mutations are especially intriguing because they present such a dramatic developmental phenotype based on a single amino acid substitution. While it is not uncommon for an amino acid substitution to have a dramatic impact on protein structure or function, the UGDH E416D and UGDH R141C mutations are somewhat unique because they lie distant from the enzyme active site and would not, on cursory examination, be expected have a significant impact on either enzyme catalysis or structure. Thus, the question arises of how these mutations affect UGDH structure and function, both *in vitro* and *in vivo*.

Kinetic characterizations have revealed that these two mutants, UGDH E416D and UGDH R141C, have essentially wild-type activity. Negligible differences in apparent K_m and V_{max} were observed. Therefore, the activity level of the mutant and wild-type enzymes in a physiological context, where substrates are more limited than in our *in vitro* characterizations, would be essentially the same unless other factors such as post-translational regulation are perturbed.

A key observation of these mutants provided a possible explanation for the observed phenotypic differences from wild-type. Gel filtration demonstrated that each of the mutant enzymes had an altered oligomeric state compared to the hexameric, wild-type enzyme. UGDH E416D eluted as a single peak representing a molecular weight of ~120KD. Compared to the

~360KD wild-type hexamer, this data clearly indicates that UGDH E416D exists as a dimer. On the other hand, UGDH R141C eluted as two nearly equal peaks of ~120KD and ~360KD, indicating that this mutant enzyme exists in an equilibrium between the dimeric and hexameric state. In fact, it is likely that at the presumably lower UGDH concentrations in the cell compared to the gel filtration study, that this equilibrium may be further shifted toward the dimeric state. Thus, while the clinical UGDH mutants do not significantly impact *in vitro* activity, they have the effect of destabilizing the interactions at the dimer-dimer interface, resulting in dimeric mutant enzymes.

It is well documented that many species suffer from developmental abnormalities when UDP-glucose dehydrogenase is mutated [11]. The effects may be severe and cause embryonic lethality as is the case when the *sugarless* gene of *D. melanogaster* contains certain mutations [11] or less severe as is the case of mutations of the *sqv-4* gene of *C. elegans* that results in defects in vulval morphogenesis [32-34]. Consistent with the work of our collaborator with human UGDH in zebra fish, mutation of the *jekyll* gene, which encodes UDP-glucose dehydrogenase, in zebra fish results in defects in heart valve formation [35]. These phenotypic developmental problems seem to be related to problems in synthesis of proteoglycans and glycosaminoglycans, which require production of UDP-glucuronate precursors by UGDH.

In the case of the clinical mutants where it has been demonstrated that *in vitro* activity of the mutant enzymes mimics activity of the wild-type

enzyme, some explanation is needed for the apparent defect in *in vivo* UGDH function suggested by a phenotype that has been linked to impaired synthesis of glycosaminoglycans. The observation that the clinical mutants have dimeric rather than hexameric structure requires further investigation into the impact of perturbation of oligomeric structure on the *in vivo* function of the enzyme.

Creation and Initial Characterization of the UGDH Engineered Dimer Mutants

To better study the effects of oligomeric state on *in vivo* UGDH regulation, we created two more UGDH dimer mutants. The experiments with the engineered dimer mutants essentially recapitulated those of the clinical UGDH dimer mutants. Both engineered mutants were found to be primarily dimeric in character. *In vitro* kinetic characterizations demonstrated that the mutants, with slight variation for UGDH E110A, possessed essentially wild-type activity.

Initially, gel filtration and analytical ultra-centrifugation (AUC) confirmed our success in creating dimeric UGDH mutants by mutating a single amino acid residue for each mutant. The gel filtration profiles were unambiguous and showed a single peak for each mutant between ovalbumin (43 KD) and aldolase (158 KD) with a molecular weight of ~120 KD, consistent with a dimer. On the other hand, the analytical ultra-centrifugation revealed more details about the proteins. While both dimer mutants were found

primarily in the dimeric state, UGDH T325A was found to have a very small second peak at the molecular weight of hexameric UGDH. Interestingly, this small amount (5% or less of the total) of hexameric T325A is not detectible by gel filtration. Similarly, wild-type UGDH has, in addition to the hexameric AUC peak, a small dimeric peak, a phenomena that has been observed multiple times by members of our lab using gel filtration.

Another interesting aspect of the AUC data is that the two engineered dimer mutants have slightly different molecular weights. UGDH E110A has a molecular weight of 137 KD, while UGDH T325A has a molecular weight of 122 KD. This difference likely reflects the destabilized, floppy structure of UGDH E110A compared to UGDH T325A, which would likely migrate more slowly through the solvent due to minor differences in shape. While UGDH E110 formed an intra-dimer hydrogen bond at the dimer interface, it also formed a hydrogen bond with another residue on the same □-helix it is positioned on (Figure 2.6). Thus, mutation to an alanine not only destabilizes the hexameric structure, it also destabilizes each monomer.

The kinetic data also demonstrate that UGDH E110A may be slightly destabilized by loss of this hydrogen bond. The mutant enzyme has approximately half the apparent V_{max} of wild-type, while the apparent K_m for UDP-glucose is increased ~ 2 fold and the apparent K_m for NAD^+ is decreased by ~1/2. This, combined with the comparatively large error bars for UGDH E110A, indicates that UGDH E110A has slightly erratic behavior due to slight

internal destabilization. In contrast, UGDH T325A is similar to UGDH E416D in that it has almost identical kinetic constants to wild-type UGDH. Therefore, we successfully created two UGDH mutants that have dimeric structure and wild-type *in vitro* activity. Thus, the engineered dimer mutants provide an ideal compliment to our study of the effects of oligomeric structure on *in vivo* UGDH function and regulation in the clinical UGDH mutants.

Comparison of UDP-glucuronate levels between wild-type and mutant UGDHs

Having assembled a set of UGDH dimer mutants, we directed our efforts at measuring UDP-glucuronate levels in human cells having either wild-type or mutant UGDH to evaluate the *in vivo* enzyme function. Many methods have been used to study intercellular glucuronate levels. Originally, thin layer chromatography allowed the identification and rough quantification of UDP-glucuronate levels [85]. Newer methods have allowed greater sensitivity and confidence in measurements, particularly high performance liquid chromatography (HPLC) and mass spectrometry [3, 84, 86-88]. While mass spectrometry is alluring, its use in metabolomics is in its infancy, and only one report of its use to measure UDP-glucuronate exists [88]. HPLC, on the other hand, has been widely used to measure UDP-glucuronate levels using both strong anion exchange and reverse phase methods [3, 84, 86, 87]. HPLC using a strong anion exchange column is

particularly well suited to measure UDP-glucuronate levels, as well as UDP-glucose, NAD^+, NADH, and other related metabolites and breakdown products. For these reasons, HPLC was utilized to assess *in vivo* UGDH function.

Our results appear to reflect the complex nature of sugar metabolism in the cell rather than the function of UGDH. The absolute value of UDP-glucuronate measured was very low, with the peak being one of the smaller peaks we were able to detect. The peak size and corresponding amount of glucuronate did not appear to depend on whether we over-expressed wild-type or mutant UGDH in the cells. The remainder of the metabolite levels, including those comparing the wild-type to the clinical mutants, varied less than 2 fold with no consistent trends in product levels or substrate levels that might be attributed to UGDH activity.

While it is disappointing that there is such little variance in UGDH substrate and product levels, it is not entirely surprising. NAD^+ and NADH are cofactors in numerous reactions in the cell, so we would not necessarily expect to see observable differences in these pools based on altering the dynamic of a single enzyme's activity. UDP-glucose is also a basic cellular metabolite with many fates other than conversion to UDP-glucuronate. For example, in the cytosol, besides conversion to UDP-glucuronate, UDP-glucose may be epimerized to UDP-galactose, used to synthesize glycogen or directly transported into the lumen of the ER or Golgi to participate in protein or lipid

glycosylation [89-91]. While glucose is rarely found in mature glycoproteins, it is used as a checkpoint sugar for proper glycoprotein folding before being removed from the mature protein [91, 92]. Recently, it has also been shown that significant levels of UDP-glucose may be released into the extracellular space and may interact with the PY2 family of receptors as a part of purinergic transmission [93-96]. With all of these fates of UDP-glucose, perhaps conversion into UDP-glucuronate is minor pathway, and UGDH activity has little overall impact on UDP-glucose levels in the cell.

A variety of reasons also exist why UDP-glucuronate levels did not vary greatly based on UGDH activity in the cytosol. First of all, UDP-glucuronate is used in the lumen of the ER or Golgi for protein glycosylation or GAG synthesis. Numerous transporters have been identified that transport UDP-glucuronate, and often other related sugars, from the cytosol into the ER and Golgi [9, 97]. Additionally, depending on cell type and environmental condition, a major fate of cytoplasmic UDP-glucuronate is conjugation to xenobiotics by UDP-glucuronosyltransferases and subsequent export from the cell [85, 98-100]. These mechanisms ensure that the levels of free UDP-glucuronate remain low in the cytosol.

Furthermore, an ever-increasing body of evidence suggests that UGDH activity is tightly regulated at both the transcriptional level and the post-translational level. UGDH is known to be transcriptionally up regulated in response to androgens in various tissue types, including the prostate

epithelium and breast cancer cells [24-26]. It has also been shown that the UGDH promoter contains a peroxisome proliferative receptor α (PPAR α) response element that mediates up regulation of UGDH in response to certain xenobiotics [27, 28].

At the post-translational level, and more directly relevant to our results, UGDH activity responds to a variety compounds. UDP-xylose has long been recognized as an effective inhibitor of UGDH function [29]. Reports suggest that UGDH is competitively and allosterically regulated by UDP-xylose [19, 29]. UDP-xylose is formed in the lumen of the Golgi and ER by UDP-xylose synthase, also known as UDP-glucuronate decarboxylase [10]. A recent study in Chinese hamster ovary cells indicates that UDP-xylose transporters transport UDP-xylose to the cytosol to inhibit UGDH activity. Consequently, loss of the UDP-xylose transporter resulted in a 200-fold increase in cellular UDP-glucuronate levels [10]. Another recent study implicates two polyphenols, gallic acid and quercetin, in inhibition of UGDH activity in the cytosol [30]. Gallic acid was found to be a non-competitive inhibitor, while quercetin showed competitive inhibition with respect to UDP-glucose and mixed-type inhibition with respect to NAD^+ [30]. A recent *in vitro* screen performed for our laboratory also identified quercetin and several other compounds having the typical polyphenol ring structure (along with numerous other non-polyphenolic compounds) as being inhibitors of UGDH activity.

Because UDGH action is potently inhibited by a down-stream product, UDP-xylose and by other naturally occurring compounds, UDP-glucuronate production is likely to be limited. Additionally, due to the presumably rapid siphoning of UDP-glucuronate to its multiple metabolic fates and the tight regulation of UGDH activity by both transcriptional and post-translational mechanisms, the levels of UDP-glucuronate in the cytosol remain at a constant, low level, as reflected in our HPLC results.

However, in spite of the lack of meaningful differences in UDP-glucuronate levels, the observed phenotype of heart valve development defects associated with the clinical UGDH mutants can be at least partially explained by differences in protein stability between wild-type UGDH and the dimeric mutants. In the *in vitro* stability assays, all four dimer mutants lost activity much more rapidly than the wild-type enzyme when incubated at 37°C. Thus, the dimer mutants may impact heart valve development by producing less UDP-glucuronate even though a comparable amount of UGDH is being produced by the cell.

In conclusion, the clinical and engineered UGDH dimer mutants were used to examine differences in *in vivo* UGDH function resulting from loss of hexameric structure. While the set of dimer mutants exhibited near wild-type activity *in vitro*, significant differences in UDP-glucuronate levels were not observed in HEK 293 cells. Despite this, the phenotype of heart development defects associated with the UGDH clinical mutants is at least partially

explained by a reduction in protein stability. Consequently, future efforts should be directed at developing new methods of effectively measuring *in vivo* UGDH activity and stability to confirm and quantify this proposed loss of activity due to protein stability.

Chapter 3

Enzymatic defects underlying hereditary glutamate cysteine ligase deficiency are mitigated by association of the catalytic and regulatory subunits

Note: The work described in this chapter has been written up for publication.

The authors and title of the paper are:

Melanie Neely Willis, Yilin Liu, Ekaterina I. Biterova , Heejeong Kim, Jaekwon Lee,

and Joseph J. Barycki. (2011) Enzymatic defects underlying hereditary glutamate cysteine ligase deficiency are mitigated by association of the

catalytic and regulatory subunits.

3.1 Introduction

Glutathione (L-γ-glutamyl-L-cysteinyl-glycine; GSH) is an abundant tripeptide critical for oxidative stress response and detoxification of xenobiotics. It contributes to signalling pathways as well as the regulation of enzymatic activity by altering the accessibility of protein sulfhydryl groups [51, 62]. In addition to serving as a redox buffer, glutathione participates in the storage and transport of cysteine [101] and select heavy metals [102]. The diverse functions of glutathione are necessary for normal cellular processes [101, 103-105], and disruption of glutathione homeostasis is associated with numerous disease states [106, 107].

Glutathione is synthesized in humans by the sequential action of glutamate cysteine ligase (GCL) and glutathione synthetase [93] [108]. GCL catalyzes the formation of an amide linkage between the γ-carboxyl group of glutamate and cysteine to form γ-glutamylcysteine, which is the rate-limiting step in glutathione biosynthesis. In vertebrate systems, GCL typically exists as a heterodimer consisting of a catalytic subunit (73 kDa) and a modifier subunit (31 kDa). The catalytic subunit (GCLC) contains the active site while the modifier subunit (GCLM) participates in regulation of enzymatic activity, enhancing catalytic efficiency upon heterodimer formation [37]. GCLC null mice are embryonic lethal [64, 105] while GCLM null mice are viable, producing low levels of glutathione (10%-20% of normal levels), consistent with a regulatory role [25].

Several reports of hereditary GCL deficiency in humans have been communicated [65-69]. The disease is marked by hemolytic anemia, low levels of erythrocyte glutathione (typically < 10% of normal levels), and in some cases, neurological disability. In the past decade, specific mutations in the coding region of GCLC have been identified in patients with hereditary GCL deficiency. Of the four clinical mutants identified thus far, three result in a leucine substitution: proline 158 (Pro158Leu), histidine 370 (His370Leu), or proline 414 (Pro414Leu). In each case, GCL activity was markedly reduced in erythrocyte samples with corresponding reductions in glutathione levels. However, the precise mechanism by which the mutation reduced enzymatic activity was not identified beyond speculation that each mutation may impact protein stability. A fourth mutation, resulting in the substitution of an arginine residue at position 127 with a cysteine residue (Arg127Cys), has been shown to directly impair enzymatic activity [66].

Recently, the crystal structure of the closely related *Saccharomyces cerevisiae* GCL was reported, allowing a credible homology model of human GCLC to be generated (Figure 1) [44]. Examination of the model provided significant insights to the possible functions of each of these four residues. In the current study, we used GCLC null mouse embryonic fibroblasts [105] and *S. cerevisiae* devoid of glutamate cysteine ligase (Δ*gsh1*) as model systems to further examine the impacts of these clinical mutations on glutathione production. In addition, we have kinetically characterized each of the human GCLC clinical mutants, either alone or in complex with human GCLM. The

results of these studies demonstrate the impact of the clinical mutations responsible for hereditary GCL deficiency on the activity of the enzyme *in vitro* and *in vivo*, as well as the critical role of the modifier subunit in enhancing wild-type activity and restoring mutant activity.

3.2 Materials and Methods

Plasmid construction and manipulations. The coding sequence corresponding to GCLM (NM_002061.2) was amplified from a human cDNA library incorporating the appropriate restriction sites into the designed primers. For expression in *S. cerevisiae,* the insert was digested with BamH1 and Xho1 and ligated into a complementarily digested p416 ADH vector [109]. The bacterial construct was generated using a pET28a vector (Novagen) and the restriction enzymes NheI and SalI. To generate expression vectors for human GCLC (NM_001498.3), the coding sequence was inserted into a p415 ADH [109], a pCMV6-Entry (C-terminal Myc and DDK Tagged), or a pET24a (Novagen) vector for expression in *S. cerevisiae*, mouse embryonic fibroblasts, or *E. coli*, respectively. The point mutations, His370Leu, Pro158Leu, Pro414Leu and Arg127Cys, were introduced using the QuikChange site-directed mutagenesis kit (Stratagene) following the manufacturer's instructions. All constructs were verified by sequencing (Eurofins MWG Operon).

Mammalian tissue culture. A GCLC null mouse embryonic fibroblast cell line, $GCLC^{-/-}$, was generously provided by Dr. Zhengzheng Shi and cultured in glutathione-containing media to 60% to 70% confluency as described previously [105]. Cells were transiently transfected with wild-type GCLC and each clinical mutant using FuGeneHD transfection reagent (Roche). After 24 hours, the media was replaced with glutathione-deficient media. Cells were

cultured an additional 24 hours, released with trypsin, and washed with cold 1X PBS. The cells were counted and evaluated by Western Blot, using polyclonal antibodies raised against full-length recombinant GCLC and GCLM (Covance). Protein levels were normalized against β-tubulin, using an Odyssey Infrared Imaging System (LI-COR) with Alexa Fluor 688 anti-mouse IgG (Invitrogen; β-tubulin) and IRDye 800 anti-rabbit IgG (Rockland; GCLC and GCLM) as secondary antibodies. Human GCLC was consistently observed as a doublet with an approximate molecular weight of 75 kDa. Both bands were used for quantification.

Determination of relative glutathione levels. To determine intercellular glutathione levels, cells were lysed by mechanical disruption (BulletBlender; Next Advance). After centrifugation, glutathione levels were quantified in the cleared lysates using an enzymatic recycling method [110] that employs glutathione reductase and 5,5'-dithio-*bis*-2-nitrobenzoic acid (Cayman Chemical Company). Glutathione levels were normalized to GCLC protein levels in the transfectants, with wild-type GCLC set equal to 1. Each transfection was performed in triplicate and the mean value and standard error for each mutant determined. Using Prism (Graphpad Software), an ANOVA one-way test with Dunett's Multiple Comparison Test was used to determine the statistical significance of the lower glutathione levels observed in the mutant transfectants.

Yeast Spotting Assay. A BY4741 haploid *S. cerevisiae* strain deficient in glutamate cysteine ligase (Δ*gsh1*; Open Biosystems) requires exogenous glutathione for growth, thus providing a powerful screening tool for the formation of functional human GCL heterodimer. Δ*gsh1* were transformed with wild-type or mutant GCLC, with or without wild-type GCLM. An empty p416ADH vector was co-transformed with the GCLC alone samples. The transformations were performed as previously described [111]. Briefly, Δ*gsh1* yeast were streaked on YPD (Yeast, Peptone and Dextrose, complete media) plates and a single colony was selected and grown overnight in liquid culture. Cells were harvested by centrifugation, washed with sterile water followed by 1X Tris-EDTA/0.2M lithium acetate, and resuspended in 1X Tris-EDTA/0.2M lithium acetate. After incubation for 15 minutes at 30°C, the plasmid constructs and 40% PEG3350/TE/0.1 lithium acetate were added to the cells. Cells were further incubated at 30°C for 20 minutes, followed by heat shock at 42°C for 20 minutes. The transformed cells were plated on uracil/leucine deficient plates (Synthetic Defined Media without leu and ura; SD-leu,ura). GCLC only tranformants grew poorly in the absence of glutathione and required the addition of 10 μM glutathione. GCLC with GCLM transformants were restreaked and grown overnight in uracil/leucine deficient media containing 1 μm glutathione. The next day, the yeast were diluted to 0.2, 0.1, and 0.04 $OD_{600\,nm}$ and spotted on uracil/leucine deficient plates. Plates were monitored for growth for 72 hours. Data for the 36 hour time point are presented.

Protein expression and purification. The initial purification steps for recombinant human GCLC and GCLM were comparable to those described for *S. cerevisiae* GCL [44]. The GCLC or GCLM construct was used to transform *Escherichia coli* Rosetta BL21(DE3) cells (Novagen). Cells were grown in 2xYT medium containing 50 μg ml^{-1} kanamycin at 30°C, and protein production was induced by the addition of 500 μM isopropyl-1-thio-β-D-galactopyranoside once the cells reached an A_{600nm} of 0.6. After induction, cultures were grown overnight at 18 °C. Cells were harvested by centrifugation (20 min, 8000 × g, 4 °C) and stored at −80 °C. Frozen cell pellets were thawed, resuspended in lysis buffer (50 mM sodium phosphate buffer, pH 8.0, 300 mM NaCl, 0.2 mM protease inhibitor, 10 mM imidazole), treated with lysozyme (1 mg/ml), and disrupted by sonication. Following centrifugation to remove cellular debris (30 min, 20,000 × g, 4 °C), the supernatant was loaded onto a HisTrap Chelating HP Column (GE Healthcare) equilibrated with lysis buffer. The column was washed to baseline (A_{280nm}), and the remaining bound proteins were eluted using a linear imidazole gradient (10–250 mM). For GCLM, appropriate fractions were pooled and required no additional purification. GCLM was dialyzed against 20 mM Tris, pH 7.4 containing 2 mM DTT, concentrated (Amicon stirred cell 8050, 10-kDa cut-off), flash-frozen in liquid nitrogen, and stored at -80°C.

For GCLC, the protein was dialyzed against 50 mM Tris, pH 8.0 containing 2 mM DTT and subjected to ion-exchange chromatography using a HiTrap Q FF column (GE Healthcare). Pooled fractions were then dialyzed

against 50 mM Tris pH 7.4, 300 mM NaCl, 2 mM DTT, and subjected to size-exclusion chromatography using a HiPrep 16/60 column Sephacryl S-100 HR column. After pooling the appropriate fractions, GCLC was dialyzed against 20 mM Tris, pH 7.4 containing 2 mM DTT, concentrated (Amicon stirred cell 8050, 10-kDa cut-off), flash-frozen in liquid nitrogen, and stored at -80°C. The holoenzyme complex was prepared by mixing purified GCLM and GCLC at a ratio of 2:1. Initially, the wild-type heterodimer was isolated from individual subunits by size-exclusion chromatography. Subsequent kinetic studies indicated that the crude 2:1 GCLM/GCLC mixture accurately reflects the catalytic efficiency of the purified heterodimer.

Kinetic assays. Enzymatic activity was measured using an indirect assay that couples ADP production to NADH oxidation [41]. Each wild-type and mutant GCLC was characterized alone or in complex with GCLM. The reaction mixture contained 20 mM $MgCl_2$, 5 mM phosphoenolpyruvic acid, 0.2 mM NADH, and 4 units each of pyruvate kinase and lactate dehydrogenase (Sigma) in 1 ml of buffer (100 mM Tris, pH 8.0, 150 mM KCl). To determine the apparent kinetic constants, two of the substrates were held at or near saturating concentrations and the third was varied. Typically, substrates were held at concentration between 5 to 10-fold over the determined K_m value. However, considerable substrate inhibition was observed with excess ATP present, similar to *S. cerevisiae* GCL [112], necessitating compromises with respect to achieving complete saturation. Thus, ATP concentrations were generally held at 3 to 5-fold over the determined K_m value to limit

substrate inhibition. Reduction in absorbance at 340 nm was followed over three minutes, and measurements were determined in triplicate. Michaelis-Menten kinetics were observed and apparent K_m and V_{max} values were determined using Prism (Graph Pad Software). To examine protein stability, human GCLC and GCLM/GCLC heterodimer (~ 1mg/mL) were incubated at 37°C. At the indicated time, an aliquot was removed and enzymatic activity assayed. The mean and standard deviation for three replicates are presented as relative activity versus time.

3.3 Results

Recapitulating homozygous mutations using a GCLC-deficient mammalian model system. To begin examining the molecular basis of human GCLC deficiency, embryonic fibroblasts obtained from GCLC null mice [105], $GCLC^{-/-}$, were transiently transfected with wild-type or mutant human GCLC. Relative GCLC expression was quantified by western analysis and normalized to β-tubulin. The hGCLC antibody, raised in rabbit against full length recombinant hGCLC, readily detected wild-type and mutant proteins, recognizing a doublet of approximately 75 kDa (Figure 3.1, inset). This doublet has been observed previously [113, 114]. The precise identity of the two species has not been demonstrated and it is unclear if these modifications impact activity. However, several reports have suggested that GCLC may be post-translationally modified [57, 113, 115]. The total glutathione concentrations for the wild-type and mutant transfectants were measured

and normalized to GCLC expression. As seen in Figure 3.1, the mean glutathione level in untransfected cells was negligible. The nominal level observed was the result of the exogenously supplied glutathione needed for growth. The untransfected (<1%) and the Pro414Leu (~37%) transfected cells had glutathione levels that were statistically reduced relative to wild-type GCLC transfectants. Glutathione levels in the His370Leu, the Arg127Cys, and the Pro158Leu transfectants were consistently reduced with levels between 60% and 70% of wild-type. These reproducible but modest reductions are in contrast to more dramatic reductions observed in patient samples. This may reflect differences in cellular GCLC:GCLM ratios as discussed below.

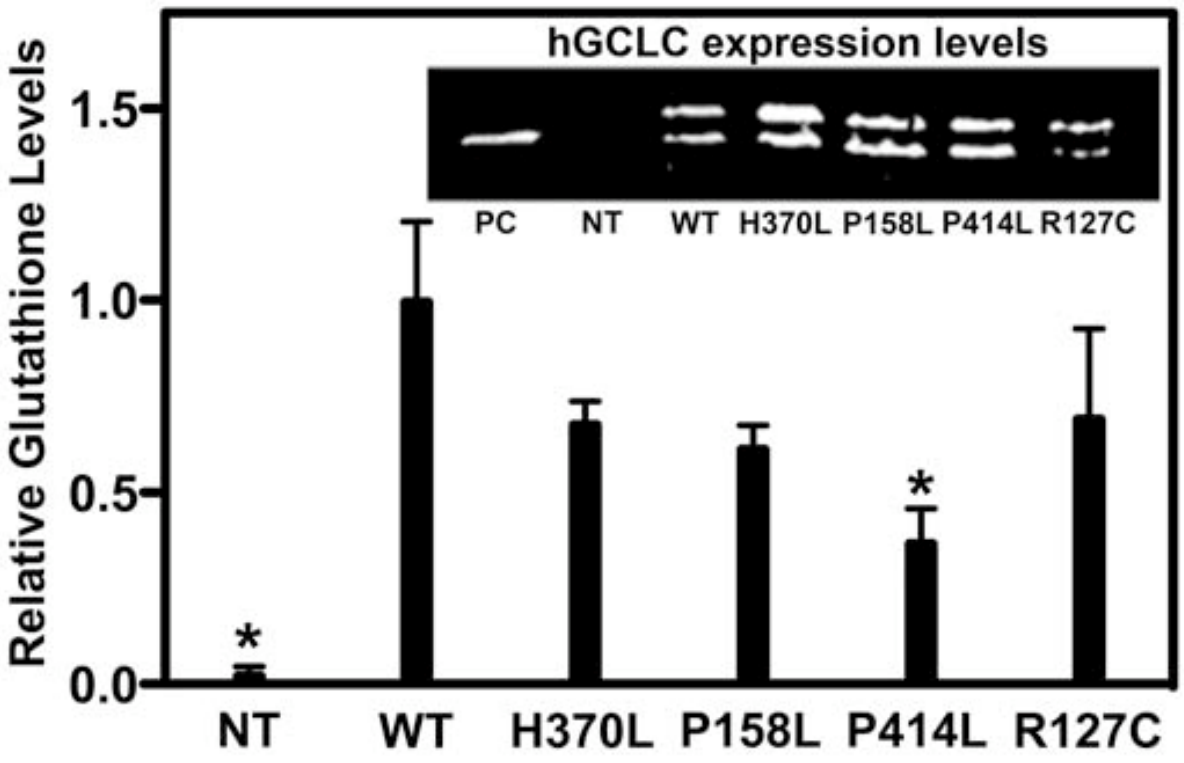

Figure 3.1. Glutathione production is reduced as a result of each of the four clinical mutations. Embryonic fibroblasts obtained from GCLC null mice were transiently transfected with wild-type or mutant human GCLC. Inset. hGCLC expression

was monitored via Western blot analysis. Purified recombinant hGCLC was used as a positive control (PC), and the non-transfected cells (NT) as a negative control. Main. Total glutathione levels were measured and normalized to protein levels, using β-tubulin (not shown) as a loading control. As discussed in the text, each mutant transfectant had reduced levels of glutathione compared to wild-type, but only the non-transfected control and the Pro414Leu transfectant were statistically lower.

Assessing the contributions of the regulatory subunit to GCL activity in an S. cerevisiae model system. In mammalian systems, GCLC and GCLM are differentially regulated and the relative ratio of the two proteins impacts overall glutathione production [37, 61, 116]. The GCLC-null mouse embryonic fibroblast cell line has a basal level of GCLM, and the heterodimer is the major species observed when GCLC is transiently expressed (data not shown). To assess the contributions of GCLM to the overall efficiency of the GCLC mutants, it was necessary to find a system in which neither GCLC nor GCLM is expressed. Since a double null GCLC/GCLM mammalian cell line is not yet available, we identified *S. cerevisiae* as an alternative eukaryotic system. *S. cerevisiae* has a single gene, *gsh1*, that is responsible for the synthesis of γ-glutamylcysteine and is closely related to human GCLC [117, 118]. The Δ*gsh1* strain is unable to produce glutathione and grows only when supplied with an exogenous source or when transfected with GCL. Thus, the Δ*gsh1* yeast line provides a reasonable system to examine the interplay between the GCLC and GCLM subunits.

The Δ*gsh1* yeast line was transformed with either wild-type or mutant GCLC and plated on the appropriate selection media (SD-leu,ura).

Overnight cultures were initiated but required the addition of 1μM glutathione to obtain a reasonable growth rate. Several dilutions of each overnight culture were spotted and monitored for growth. Although protein expression levels for wild-type and GCLC mutants were comparable, wild-type GCLC could only weakly rescue the Δ*gsh1* strain whereas none of the mutant GCLC transformants grew (Figure 3.2), consistent with impaired function. Co-expression of wild-type GCLC and GCLM resulted in robust growth as a result of increased glutathione synthesis. Strikingly, co-expression of GCLM with Pro158Leu restored growth to levels comparable to wild-type holoenzyme. To a lesser degree, the addition of GCLM partially rescued the Arg127Cys and the His370Leu mutants. In contrast, the Pro414Leu mutant, either alone or co-expressed with GCLM, did not grow without the addition of reduced glutathione.

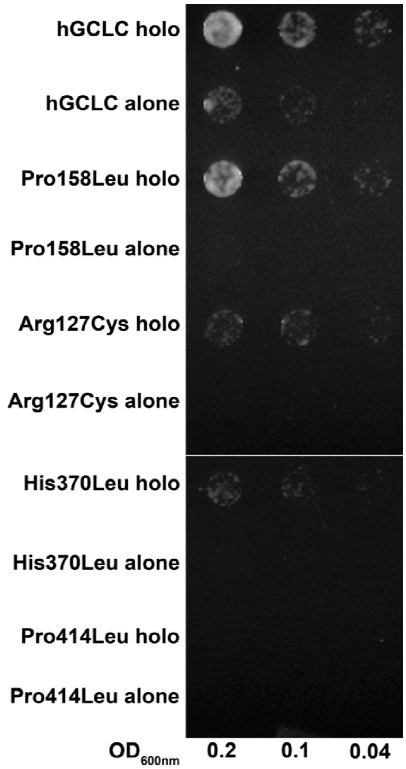

Figure 3.2. The modifier subunit enhances the activity of wild-type and mutant hGCLC. An *S. cerevisiae* strain deficient in glutamate cysteine ligase (ΔGSH1) was transformed with wild-type or mutant GCLC, with or without wild-type GCLM. An empty p416ADH vector was co-transformed with the GCLC alone samples. Transformants were restreaked, grown overnight in uracil/leucine deficient media, diluted to 0.2, 0.1, and 0.04 $OD_{600\ nm}$, spotted on uracil/leucine deficient plates, and grown for 72 hours as described in the text. Wild-type hGCLC alone could complement but more robust growth was observed when the holoenzyme was present. None of the four mutant hGCLC transformants grew under these conditions. However, formation of the holoenzyme restored near wild-type growth to Pro158Leu, and permitted limited growth of Arg127Cys and His370Leu. However, addition of the modifier subunit did not impact growth of the Pro414Leu mutant.

Characterization of recombinant human GCLC and GCLM. To further dissect the impacts of human GCLC mutations on enzymatic function, each protein was overexpressed in *E. coli* and purified to homogeneity (>95% pure based on SDS-PAGE). Typical yields were ~50 mg/L of bacterial culture for human

GCLM and ~10 mg/L of bacterial culture for human GCLC. Similar yields were observed for each of the four clinical mutants, suggesting that overall protein folding was not dramatically compromised by the mutations. Apparent steady state kinetic constants for the catalytic subunit alone (Table 3.1) and the holoenzyme (Table 3.2) were determined using a coupled assay system that monitored the production of ADP as a measure of enzymatic activity.

Human GCLC had kinetic constants within the range of activities reported previously [37, 55, 116, 119, 120]. The formation of the GCLM/GCLC heterodimer increased V_{max} while significantly reducing the apparent K_m value for ATP and to a lesser extent, the K_m for glutamate (compare columns 1 and 3 in Tables 3.1 and 3.2) [116]. Noticeable substrate inhibition was observed at increasing concentrations of cysteine or ATP, with estimated K_i values of 10 – 15 mM and 2 – 4 mM respectively (data not shown). The high concentrations of ATP used for K_m determinations consistently impacted the observed enzymatic rates and accounted for the slight variability in the observed V_{max} values. Therefore, all comparisons of enzymatic activity used V_{max} values determined as a function of ATP concentration. The Pro158Leu mutant had modest impact on the enzymatic activity of the catalytic subunit, whereas the Arg127Cys GCLC mutant reduced V_{max} by approximately 2-fold (Table 3.1). Both mutations slightly increased the apparent K_m for ATP. The His370Leu and the Pro414Leu mutants exhibited severely impaired ATP binding, with a near linear dependence of rate with respect to ATP concentration over the

range tested (data not shown). Each mutant had an estimated K_m value for ATP greater than 20 mM, precluding the accurate determination of the apparent kinetic constants for the remaining substrates.

Table 3.1. Apparent kinetic constants for wild-type and mutant human GCLC

	Glutamate		Cysteine		ATP	
	K_m (mM)	V_{max} (μmol min^{-1} mg^{-1})	K_m (mM)	V_{max} (μmol min^{-1} mg^{-1})	K_m (mM)	V_{max} (μmol min^{-1} mg^{-1})
Wild-type	1.14 ± .07	1.00 ± .019	0.10 ± .02	1.41 ± .057	2.68 ± .19	1.43 ± .047
Pro158Leu	0.68 ± .09	1.18 ± .005	0.08 ± .01	1.78 ± .047	3.57 ± .21	2.13 ± .061
Arg127Cys	1.38 ± .14	.544 ± .019	0.05 ± .01	.676 ± .014	4.47 ± .56	.837 ± .057
His370Leu	ND[a]	ND	ND	ND	ND	ND
Pro414Leu	ND[a]	ND	ND	ND	ND	ND

[a] The His370Leu and Pro414Leu mutations exhibit severely compromised ATP binding, as reflected in highly elevated K_m values for ATP. A lower estimate for each of the K_m values is approximately 20 mM, but may be considerably higher. This deficiency precluded further detailed steady-state kinetic characterizations. At a given assay condition (5 mM ATP, 10

mM Cys, 20 mM Glu, and 20 mM $MgCl_2$), the His370Leu and Pro414Leu mutants have activities that are 39% and 16% of wild-type GCLC respectively.

Formation of the activated heterodimer had differing effects on each of the four clinical mutants. For the Pro158Leu mutant, addition of GCLM increased V_{max} by approximately 2-fold while significantly lowering the apparent K_m for ATP, similar to wild-type enzyme (Table 3.2). Modest effects were observed with respect to K_m values for the cysteine and glutamate substrates. For the Arg127Cys mutation, formation of the GCLM/GCLC heterodimer resulted in an increase in catalytic activity to a level comparable to wild-type enzyme. Similarly, the addition of GCLM to either His370Leu or Pro414Leu dramatically increased enzymatic activity to near wild-type levels (Table 3.2), primarily by restoring robust binding of ATP. These *in vitro* kinetic characterizations suggest that formation of the GCLM/GCLC heterodimer would mitigate the detrimental effects of the GCLC clinical mutations.

Table 3.2. Apparent kinetic constants for wild-type and mutant human GCLC/GCLM complex

	Glutamate		**Cysteine**		**ATP**	
	K_m (mM)	V_{max} (μmol min^{-1} mg^{-}	K_m (mM)	V_{max} (μmol min^{-1} mg^{-}	K_m (mM)	V_{max} (μmol min^{-1} mg^{-}

		[1])		[1])		[1])
Wild-type	0.46 ± .08	1.21 ± .061	0.07 ± .01	1.23 ± .043	0.44 ± .08	2.38 ± .260
Pro158Leu	0.65 ± .06	3.31 ± .085	0.17 ± .02	3.17 ± .085	0.30 ±.05	4.77 ± .440
Arg127Cys	1.38 ± .14	1.38 ± .052	0.12 ± .01	1.34 ± .028	0.50 ± .09	1.67 ± .170
His370Leu	0.44 ±.04	1.22 ±.028	0.16 ± .02	1.44 ± .047	0.26 ± .04	1.89 ± .166
Pro414Leu	0.77 ± .09	.913 ± .038	0.17 ± .02	.619 ± .024	0.82 ± .29	1.71 ± .426

This concept was further supported by the enzymatic stability assays (Figure 3.3). For the catalytic subunit alone, the wild-type enzyme retains nearly full activity over a 24 hour period. In contrast, the Pro414Leu and the His370Leu mutants lost more than 50% activity and the Arg127Cys and Pro158Leu mutants lost more than 95% activity over the same time. Thus, although the Pro414Leu and the His370Leu mutants were compromised catalytically (Table 3.1), they were considerably more stable than the Arg127Cys and Pro158Leu mutants, which had significantly higher enzymatic activity. The addition of the modifier subunit dramatically increased protein stability for the His370Leu, Arg127Cys, and Pro158Leu mutants. However, formation of the Pro414Leu heterodimer provided only modest stabilization.

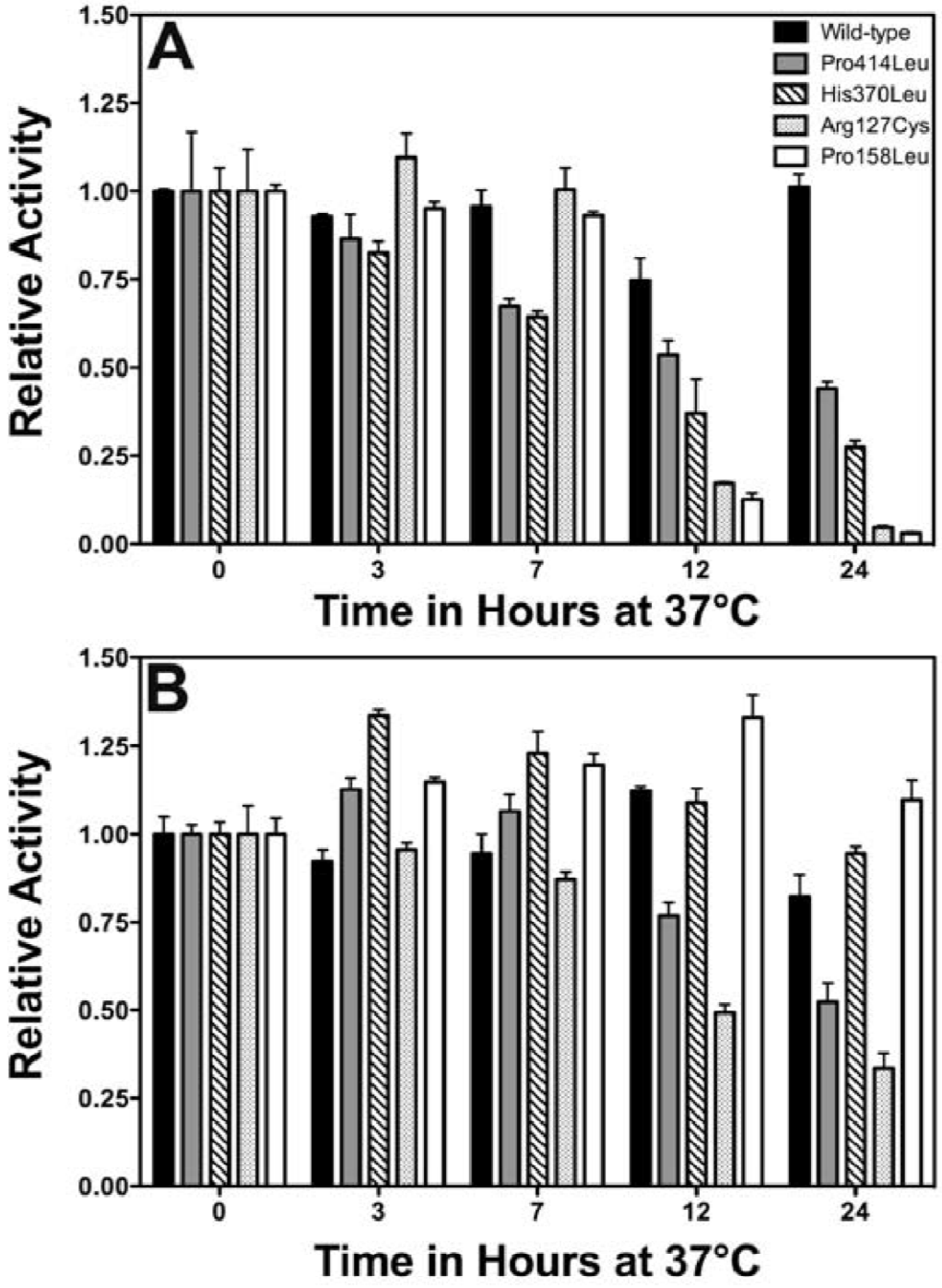

Figure 3.3. Clinical mutations destabilize overall GCLC protein stability. Wild-type and mutant GCLC were incubated at 37 °C and relative enzymatic activity was monitored as a function of time. Bars are shaded as follows: Wild-type, black; Pro414Leu, grey; His370Leu, hatched; Arg127Cys, dotted; Pro158Leu, white. **Panel A. Human GCLC in the absence of GCLM. Panel B. Human GCLC in the presence of GCLM.**

3.4 Discussion

Hereditary GCL deficiency presents a unique opportunity to examine both the molecular mechanism of the disease and the importance of the modifier subunit to the activity of the holoenzyme. Glutathione plays a central role in protecting the cell from endogenous and exogenous threats through oxidative stress remediation and xenobiotic detoxification. The importance of GCL in catalyzing the first and rate-limiting step of glutathione biosynthesis is widely recognized. However, the molecular details of catalysis and the mechanism by which association of the catalytic and modifier subunits enhances catalytic efficiency remain unclear. In the current study, four GCLC missense mutations that result in hereditary glutathione deficiency have been characterized. This work details the molecular basis of this disease and demonstrates the critical role of the modifier subunit in rescuing the activity of severely comprised mutant catalytic subunits.

To provide a quantitative assessment of the differences in glutathione production between the GCLC mutants, we transiently transfected mouse embryonic fibroblast cells from GCLC null mice ($GCLC^{-/-}$) [105]. Consistent with previous studies in which individual clinical mutations were identified [65, 66, 68, 69], each of the four mutants had lower levels of total glutathione compared to the wild-type GCLC transfectant (Figure 3.1). However, overall reductions in glutathione levels were not as dramatic as observed in patient samples. In part, this is may be due to the presence of significant quantities

of GCLM in the GCLC$^{-/-}$ cells, which stimulates glutathione production. GCLM levels were not reported for the patient samples and it is possible that GCLM levels are considerably higher in the cell culture model. However, the overall trend in relative glutathione levels is consistent with previous clinical studies.

To assess the contributions of GCLM to catalytic activity in a eukaryotic system, an *S. cerevisiae* model was employed. *S. cerevisiae* has a single gene responsible for the efficient biosynthesis of γ-glutamylcysteine, *gsh1*, and lacks a functional equivalent of GCLM [118]. Δ*gsh1* yeast transformed with either GCLC alone or with both GCLC and GCLM grew on glutathione deficient media, though the presence of GCLM conferred a distinct growth advantage (Figure 3.2). These results are consistent with observations in mice that GCLM is non-essential but enhances glutathione production [104, 116]. Unlike wild-type GCLC, none of the four mutant GCLC subunits identified in hereditary GCL deficiency patients grew in the absence of GCLM, suggesting that overall cellular glutathione levels were likely below 1 μM, the minimal level of exogenous glutathione needed to confer growth to the Δ*gsh1* strain. In contrast, the presence of GCLM was able to restore growth to three (His370Leu, Pro158Leu, Arg127Cys) of the mutant GCLC transformants. The fourth mutant, Pro414Leu, failed to grow, and is consistent with the more dramatic reduction in glutathione levels observed in the GCLC$^{-/-}$ cell culture system (Figure 3.1). Thus, the role of the modifier

subunit in enhancing catalytic activity appears to be particularly relevant in cases where the catalytic subunit is compromised by a mutation.

Based on the observed differences between wild-type and mutant GCLC in the Δ*gsh1* yeast and GCLC$^{-/-}$ cells, we performed *in vitro* kinetic characterizations in the absence (Table 3.1) and presence (Table 3.2) of the modifier subunit to further understand the impact of each amino acid mutation on enzyme catalysis and the molecular basis of disease. Consistent with earlier observations with mouse GCL [116], our kinetic studies demonstrate that the modifier subunit enhances the activity of the wild-type subunit and dramatically lowers the K_m for ATP. Strikingly, each of the mutant GCLC proteins also displayed increased activity when combined with GCLM, often attaining apparent constants comparable to the wild-type enzyme (Compare Tables 3.1 and 3.2). In addition, heterodimer formation improved the protein stability of each mutant (Figure 3.3). This suggests that therapeutics that promote heterodimer formation *in vivo* or can mimic the effects of modifier subunit binding may provide effective treatments for GCL deficiency.

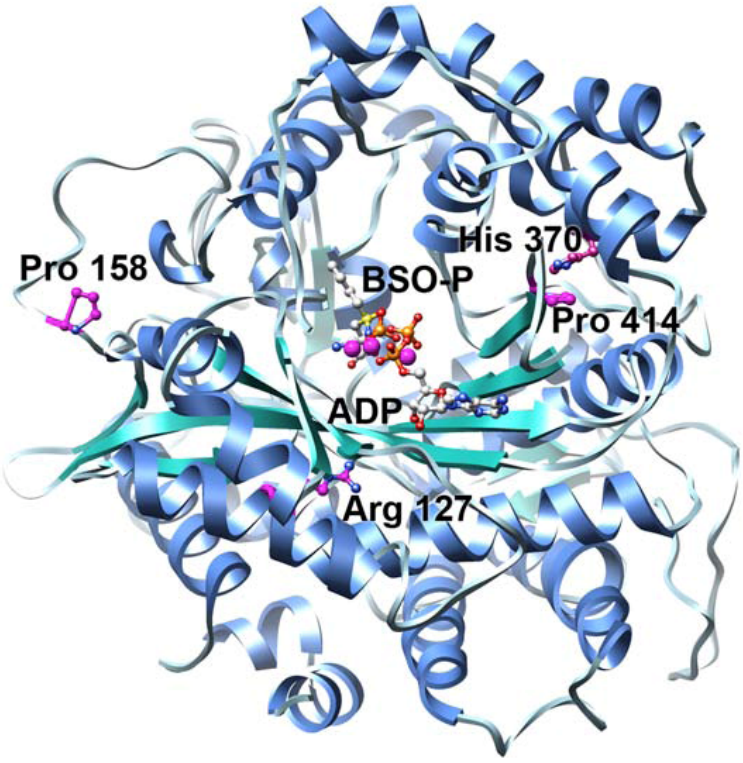

Figure 3.4. Homology model of human glutamate cysteine ligase reveals the locations of the four clinical mutations. The overall model of hGCLC is shown in ribbon representation with β-strands colored in green, α-helices in blue, and loop regions in grey. ADP and the transition state analogue, phosphorylated BSO (BSO-P), were docked into the previously described model and are shown in ball and stick representation. Carbon atoms colored in grey, oxygen atoms in red, sulfur atoms in yellow, nitrogen atoms in blue, phosphorus in orange, and magnesium atoms in purple. The locations of the four clinical mutations are highlighted, with carbon atoms colored in purple.

To understand the molecular basis of the observed kinetic and phenotypic differences, we examined a homology model of human GCLC (Figures 3.4 and 3.5) [44]. Previous modeling studies suggested that Arg 127 was located proximal to the substrate binding pocket, in a surface exposed pocket [66]. However, these studies necessarily used a more distant homologue as a template. Based on the x-ray structure of the closely related *S. cerevisiae* GCL, a more robust human GCLC homology model was

generated. In our model, Arg 127 is adjacent to the enzyme active site and forms a salt-bridge with Asp 49, as well as a hydrogen bond with the backbone carbonyl oxygen of Gly 104 (Figure 3.5A). Replacement of Arg 127 with a cysteine residue would disrupt this hydrogen bond network and negatively impact catalysis both directly and indirectly. The backbone carbonyl of Asp 49 is positioned to form a hydrogen bond with the 3′ hydroxyl group of the ATP ribose. In addition, the β-strands containing Asp 49 and Gly 104 contain conserved glutamate residues critical to function. Disruption of the Arg 127/Asp 49 salt bridge may lead to displacement of Glu 50 and Glu 52, whereas eliminating the Arg 127/Gly 104 hydrogen bond could alter the position of Glu 103. Each of these glutamate residues is involved in magnesium coordination and substrate binding, and is critical for efficient catalysis. Importantly, each of these proposed interactions is conserved in the *S. cerevisiae* GCL template [44, 112].

The predicted impacts of the Arg127Cys mutation based on modeling studies are supported by the available kinetic data. The initial report of this clinical mutation indicated that the Arg127Cys mutant alone had <5% of wild-type activity and bound glutamate and aminobutyrate, a cysteine surrogate, more efficiently [66]. However, ATP binding was not examined. In the current study, the Arg127Cys mutant in the absence of GCLM has an elevated K_m for ATP and a reduced V_{max} as compared to wild-type GCLC alone (Table 3.1), consistent with a more modest perturbation of the active site architecture. Differences in assay conditions including assay temperature,

substrate concentrations used, and the location of the engineered histidine tag used for affinity purification may account for these differences. Nonetheless, both reports demonstrate that the Arg127Cys negatively impacts catalysis. Addition of GCLM to Arg127Cys restores enzymatic activity, with the mutant holoenzyme exhibiting kinetic constants comparable to the wild-type heterodimer (Table 3.2). This restoration of Arg127Cys activity by GCLM is also evident in the yeast spotting assay in which Arg127Cys alone did not grow, but addition of GCLM permitted growth, albeit at a reduced level compared to wild-type (Figure 3.1). Similarly, the levels of glutathione found in the $GCLC^{-/-}$ cell line transiently transfected with Arg127Cys were consistently lower than wild-type glutathione levels (Figure 3.1). These observations indicate that the Arg127Cys mutation destabilizes overall protein structure, and that the additional stabilization afforded by heterodimer formation can offset these negative consequences (Figure 3.3). Thus, the addition of the modifier subunit can partially restore Arg127Cys activity, both *in vitro* and *in vivo.*

Our model of human GCLC suggests that histidine 370 and proline 414 are located in close proximity to the ATP-binding region of the active site (Figure 3.5B). Specifically, both residues appear to be involved in the positioning of a β-strand containing Lys 412, which participates in an extensive hydrogen bond network that is involved in ATP binding and proper orientation of active site residues. The mutation of proline 414 to leucine probably destabilizes a rigid series of proline residues connecting two beta

strands resulting in reduction of ATP binding. This is in contrast to a previously reported model that indicated Pro 414 was located at the end of an α-helix, considerably removed from the enzyme active site [68]. Histidine 370 appears to participate in an extensive hydrogen bond network with tyrosine 266 and glutamine 402 near the phosphate coordination region. Both His370Leu and Pro414Leu have compromised enzymatic activity in the absence of GCLM, primarily as a consequence of poor ATP binding (Table 3.1). However, addition of GCLM to either mutant rescues enzyme activity through restoration of efficient ATP binding (Table 3.2) and to different extents, improving overall protein stability (Figure 3.3). The His370Leu mutant regains near full activity whereas the Pro414Leu mutant has somewhat reduced activity. In support of this interpretation, initial studies with a Lys412Ala mutant indicate that the enzyme has severely compromised catalytic activity (MNW and JJB, unpublished observation). Overall, our data suggest that formation of the heterodimer can compensate for these destabilizing mutations by ordering the enzyme active site.

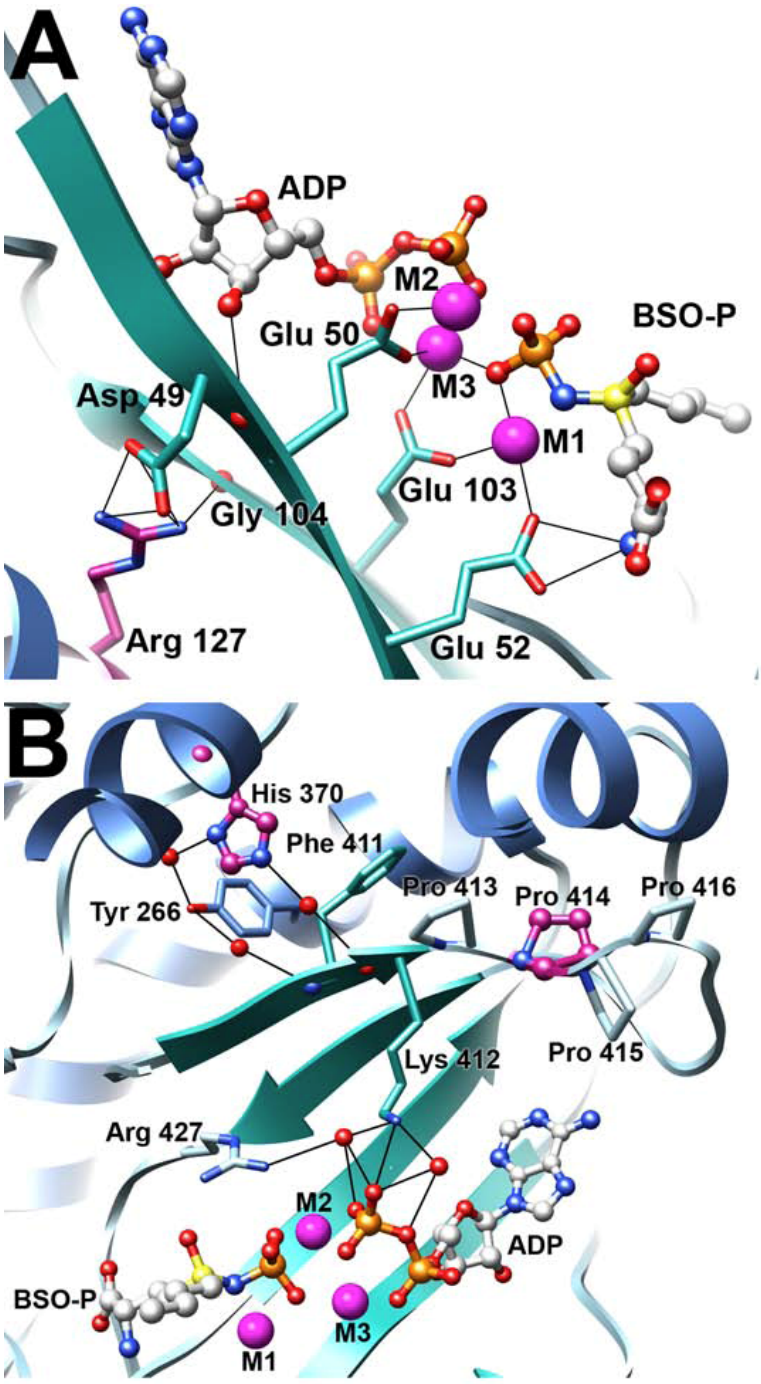

Figure 3.5. Clinical mutations disrupt hydrogen bond networks that stabilize the enzyme active site. The figure illustrates the hydrogen bond networks centered about three of the clinical point mutations. Atoms are colored as in Figure 10 with potential hydrogen bonds illustrated as solid black lines. **Panel A.** Arg 127 stabilizes two β-strands within the active site, forming a salt bridge with Asp 49 and a hydrogen bond with the backbone carbonyl of Gly 104. **Panel B.** His 370 is involved in a hydrogen bond network that positions a β-strand that contains Lys 412. Pro 414 is the second of four proline residues in a rigid loop immediately adjacent to Lys 412, which is involved in orienting the β-phosphate of ATP.

These kinetic characterizations agree with the described cell culture studies. Particularly striking is the observation that the most kinetically crippled mutant, Pro414Leu (Table 3.1), is also the only mutant that failed to grow in combination with GCLM in the yeast spotting assay and that had statistically lower glutathione levels than wild-type in the $GCLC^{-/-}$ cell-based assays. Intriguingly, the only reported clinical case of GCL deficiency with the Pro414Leu mutation was accompanied by progressive motor neuropathy of the lower extremities and psychomotor development [68]. Although other cases of neuropathy have been found in patients with GCL deficiency, the suggestion that the Pro414Leu mutation may lead to a more severe version of the disease is consistent with our experimental results.

Proline 158 lies on a solvent-exposed loop far from the enzyme active site. Its remote location and lack of sequence conservation suggests that a mutation of proline 158 to leucine would not have dramatic impact on enzyme catalysis. Our kinetic studies show that this mutation causes a slight, but distinct, increase in GCLC activity in both the catalytic only and holoenzyme forms compared to wild-type (Tables 3.1 and 3.2). In contrast, the Pro158Leu mutant exhibited reduced glutathione levels in the $GCLC^{-/-}$ cell line and could not complement the Δ*gsh1*strain, unless the modifier subunit was also present. Once the holoenzyme was formed, the growth of Pro158Leu appeared very similar to that of wild-type GCLC/GCLM heterodimer. This phenotype is very similar to that of Cys152Ala, another mutant in this region of the enzyme recently characterized by our lab (YL and JJB, manuscript in

preparation), suggesting that this region of GCLC is particularly sensitive to perturbations.

The apparent inconsistency between limited effect of the clinical mutations on apparent kinetic constants and the significant reduction in glutathione in the yeast and mouse embryonic fibroblast models can be reconciled if cellular protein stability is considered (Figure 3.3). The Pro158Leu mutant alone was the least stable enzyme of those tested. However, once the GCLM subunit was added, protein stability improved dramatically, to levels comparable to wild-type heterodimer. This suggests that the mutant catalytic subunit alone is less persistent *in vivo* perhaps due to decreased stability or increased turnover. Formation of the heterodimer stabilizes the Pro158Leu mutant and allows for the production of glutathione. This is supported by recent studies of the Pro158Leu mutant in which specific activities were measured at 37°C [121]. A dramatic decrease in Pro158Leu activity in the absence of GCLM was observed (<10% activity) as compared to wild-type enzyme. The addition of GCLM significantly stimulated activity, such that the mutant heterodimer was only approximately 4-fold less active than the wild-type holoenzyme.

Dalton and co-workers have demonstrated that erythrocyte glutathione levels are low in $GCLM^{-/-}$ mice and that GCLM is limiting in most tissues [104, 116]. Depending on tissue type, GCLC to GCLM ratios of 1.5 to 7 were typically observed, but the study did not specifically examine the GCLC/GCLM

ratio in erythrocytes. However, the observed manifestations of hereditary GCL deficiency combined with the studies reported herein are consistent with limiting GCLM in red blood cells. Patients with GCLC deficiency have very low levels of erythrocyte glutathione and exhibit hemolytic anemia, indicating that glutathione biosynthesis is compromised most notably in erythrocytes, cells in which it is needed to effectively combat oxidative stress. Our kinetic data indicate that for each mutant, formation of the heterodimer dramatically restores GCL activity. These observations suggest that GCLM may be limiting in red blood cells, such that near wild-type enzymatic activity is not realized. In addition, the mutant GCLC may not persist throughout the approximately 120 day lifespan of an erythrocyte [122] when GCLM is limiting.

In summary, our characterizations of the four clinical mutations identified in hereditary GCL deficiency reveal disparate molecular mechanisms that impair glutathione production by reducing the activity of the catalytic subunit of GCL. The critical role of the modifier subunit in enhancing activity of the catalytic subunit is evident in the ability of the modifier subunit to rescue activity of the mutant catalytic enzymes in both our *in vitro* and *in vivo* studies. Therapeutic strategies that stimulate GCLM production, stabilize the heterodimer, or mimic heterodimer formation may be effective in the treatment of this disease.

Chapter 4

Conclusions and future directions

4.1 Conclusions

UDP-glucose dehydrogenase

UDP-glucose dehydrogenase catalyzes the conversion of UDP-glucose to UDP-glucuronate via two successive oxidations, concomitantly converting two molecules of NAD^+ to NADH. UDP-glucuronate is an essential precursor for protein glycosylation, production of extracellular matrix proteins and is necessary for cellular detoxification of xenobiotics and endobiotics via UDP-glucuronosyltransferases [8, 20]. Availability of UDP-glucuronate and UGDH expression have been implicated in a variety of epithelial cancers and in developmental abnormalities [70-76]. Therefore, a detailed understanding of the structure, function, and regulation of UGDH is essential.

While UDP-glucuronate is implicated in a variety of cellular processes, recent advances in understanding both developmental abnormalities and cancer progression associated with UGDH have highlighted the role of hyaluronan, a key extracellular matrix polysaccharide in causation of both processes [75]. The common link between development and cancer progression appears to be hyaluronan's promotion of cell migration and proliferation. While the types of cancer associated with increased hyaluronan production include breast, head and neck, ventricle, colon, and pancreas cancer [31], hyaluronan and UGDH have received significant attention in prostate cancer progression, and UGDH has been named as a potential

biomarker for prostate cancer [77]. While much has already learned about UGDH, these advances demonstrate the necessity of fully delineating the many factors that control UGDH function in the cell.

Consequently, in the past decades, detailed studies have illuminated the key details of the mechanism of UGDH. More recently, advances have been made in understanding the transcriptional and post-translational regulation of UGDH. Indeed, many of these regulatory mechanisms are congruent with our current understanding of the important roles UGDH enacts in cellular metabolism. For example, UGDH is post-translationally inhibited by the downstream product UDP-xylose, which is formed in the ER or Golgi lumen by UDP-glucuronate decarboxylase, allowing feedback inhibition by the glycosylation pathway [10]. Likewise, transcriptional up-regulation of UGDH by certain xenobiotics integrates UDP-glucuronate production and cellular detoxification [28]. However, less is known about other regulators, such as gallic acid and quercetin [30]. Neither is it known whether these *in vivo* regulators are impacted by the oligomeric structure of UGDH.

Recently identified human UGDH mutants, E416D and R141C, were found to exist wholly or partially as dimers, although wild-type UGDH is a hexamer. This change in oligomeric structure was found to not significantly impact *in vitro* catalysis. However, these UGDH mutations were associated with congenital heart defects in humans and defects in cardiac valve formation in zebrafish. Therefore, we endeavored to discover whether

oligomeric state alone impacted *in vivo* UGDH function by measuring UDP-glucuronate levels from HEK293 cells transiently transfected with mutant and wild-type UGDH. In order to separate effects of the individual mutations from those dependent on oligomeric state, we engineered two more UGDH mutants that were exclusively dimers: UGDH E110A and UGDH T325A.

Presumably due to the tight regulation of UGDH and its participation in many diverse cellular processes, UDP-glucuronate levels were maintained at a low level in the cell compared to other related metabolites. No significant differences were found in levels of UDP-glucuronate, UDP-glucose, NAD^+, or NADH between wild-type UGDH and any of the mutant UGDH proteins. Thus, the development of alternative methods to measure UDP-glucuronate synthesis *in vivo* are necessary.

In spite of this, the *in vitro* stability assays demonstrate that UDP-glucose dehydrogenase activity is reduced in the dimeric mutants at 37°C. A destabilization of protein structure and activity in the clinical mutants provides a plausible explanation for the observed phenotype of developmental heart defects. During development, the demand for hyaluronan and UDP-glucuronate are elevated, so any alteration of protein stability might produce a dramatic effect not detected in the in *vivo cell* culture assays we performed. With the development of better detection methods, perhaps differences in UGDH function due to protein stability could be measured even in a cell culture model.

Glutamate Cysteine Ligase

Glutamate cysteine ligase (GCL) is a cytosolic protein responsible for the first and rate-limiting step of glutathione biosynthesis [37, 108]. Glutamate cysteine ligase catalyzes the formation of an amide linkage between the γ-carboxyl group of glutamate and cysteine to form γ-glutamylcysteine [37, 50]. In humans and other higher eukaryotes, GCL is composed of heavy catalytic subunit (73 KD) and a light modifier subunit (30 KD). The catalytic subunit is sufficient for catalysis, while the modifier subunit is known to enhance the activity of the catalytic subunit [40, 41].

Glutathione (L-γ-glutamyl-L-cysteinyl-glycine; GSH) is an abundant tripeptide critical for oxidative stress response and detoxification of xenobiotics. It contributes to signalling pathways as well as the regulation of enzymatic function by altering the accessibility of protein sulfhydryl groups [51, 80] and participates in the storage and transport of cysteine [101] and select heavy metals [102]. The diverse functions of glutathione are necessary for normal cellular function [101, 103-105], with disruption of glutathione homeostasis associated with numerous disease states, including cancer, neurodegenerative diseases, anemia, cystic fibrosis, HIV, and aging [106, 107].

Recently, four single amino acid mutations in the catalytic subunit of glutamate cysteine ligase were identified in patients with hereditary glutathione deficiency, a disease characterized by extremely low levels of erythrocyte glutathione, hemolytic anemia and neurologic problems [65-69].

We comprehensively characterized these mutant GCLC subunits, *in vitro* and in two eukaryotic systems to determine the molecular basis for disease.

By measuring the glutathione produced by each mutant GCLC in combination with the modifier subunit in mouse embryonic fibroblast cells, we demonstrated that each of the GCLC clinical mutants has lower glutathione levels than wild-type. Our yeast transformations of each mutant GCLC, both with and without the modifier subunit, highlighted the requirement of the modifier subunit for glutathione production in the mutant GCLC transformants. The *in vitro* kinetic characterizations confirmed that for 3 of the clinical mutants—P414L, H370L and R127C—the addition of the modifier subunit dramatically rescues impaired catalytic function.

Curiously, the fourth mutant, P158L, has distinctively higher activity than wild-type in both the catalytic only and holoenzyme assays. In spite of this, GCLC P158L failed to grow without addition of the modifier subunit in yeast and had a lower level of glutathione compared to wild-type in the presence of the modifier subunit in the mouse embryonic fibroblast cells. This paradox, combined with the results from the other 3 mutants showing more dramatic *in vivo* phenotypes than the kinetic data alone would suggest, indicate that some other factor affects *in vivo* functioning of the mutant enzymes compared to the wild-type. The *in vitro* protein stability assay demonstrated that each of the four GCLC mutants suffered from a dramatic loss of activity over 24 hours, while the wild-type enzyme retained full

activity, suggesting that the *in vivo* functioning of the GCLC mutants is negatively impacted by reduced protein stability. Thus, our studies of the GCLC clinical mutants indicate both the impaired catalytic function underlying hereditary glutathione deficiency and the critical role of modifier subunit in rescuing the function of these detrimental mutations.

4.2 Future Directions

UDP-glucose dehydrogenase

Our studies of UDP-glucose dehydrogenase highlight several areas where further study is merited. First of all, the *in vitro* stability assay for both the clinical and engineered dimer mutants indicate that the dimeric mutants exhibit reduced activity over time at 37°C compared to wild-type. While this suggests that protein stability may be responsible for the clinical phenotype, confirmation of *in vivo* protein stability for wild-type and each dimeric mutant would strengthen this assertion. By using a protein synthesis inhibitor such as cyclohexamide, the degradation rate of each transiently transfected UGDH protein can measured. After transfection and expression of the protein, cyclohexamide is added to prevent continuous protein synthesis. The depletion of each UGDH protein can then be measured at various time points by Western blot to establish an *in vivo* protein half-life for each mutant and wild-type UGDH.

Additionally, our measurements of UDP-glucuronate in HEK 293 cells transiently transfected with mutant and wild-type UGDH did not show any significant differences in UDP-glucuronate levels, even between the catalytically inactive mutant UGDH D280N and wild-type (Figure 4.1). In fact, UGDH D280N had 1.78 times the amount of UDP-glucuronate as wild-type, a counter-intuitive, if not significant result. While this is disappointing, the comparably low levels of UDP-glucuronate detected indicate that this metabolite is rapidly funneled to its many cellular fates and/or tightly regulated by regulation of UGDH activity.

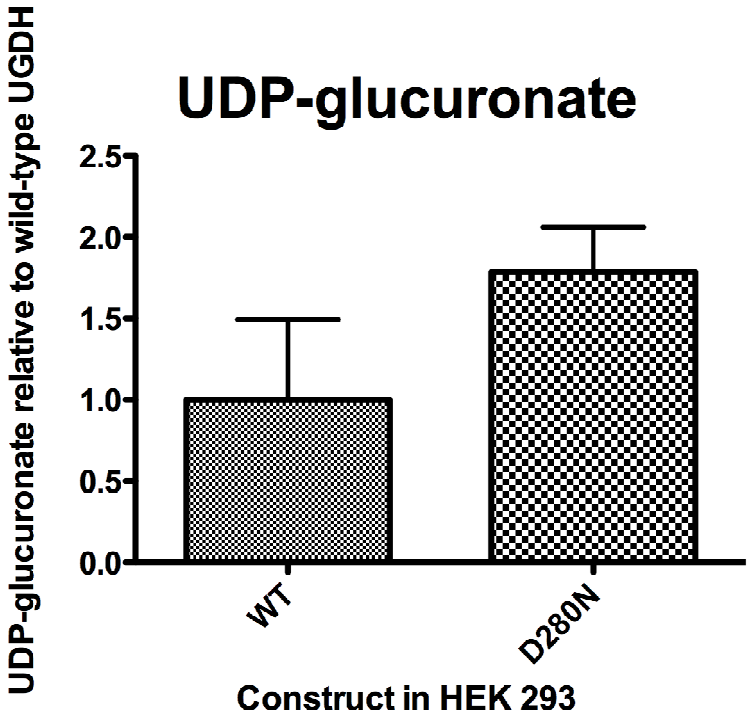

Figure 4.1. Levels of UDP-glucuronate in HEK 293 cells. HEK 293 cells were transiently transfected with each construct. UDP-glucuronate levels were measured by HPLC and normalized to total protein levels. Wild-type level is set equal to one for ease of comparison. Error bars represent the SEM of three replicates. Control and GFP values have been omitted.

However, one unexpected and intriguing result from the HPLC data is the presence of higher amounts of uridine monophosphate (UMP) in the dimeric mutant transfected cells compared to the wild-type transfected cells. The levels of UMP were 2 to 5 times higher in the mutants compared to wild-type (Figure 4.2).

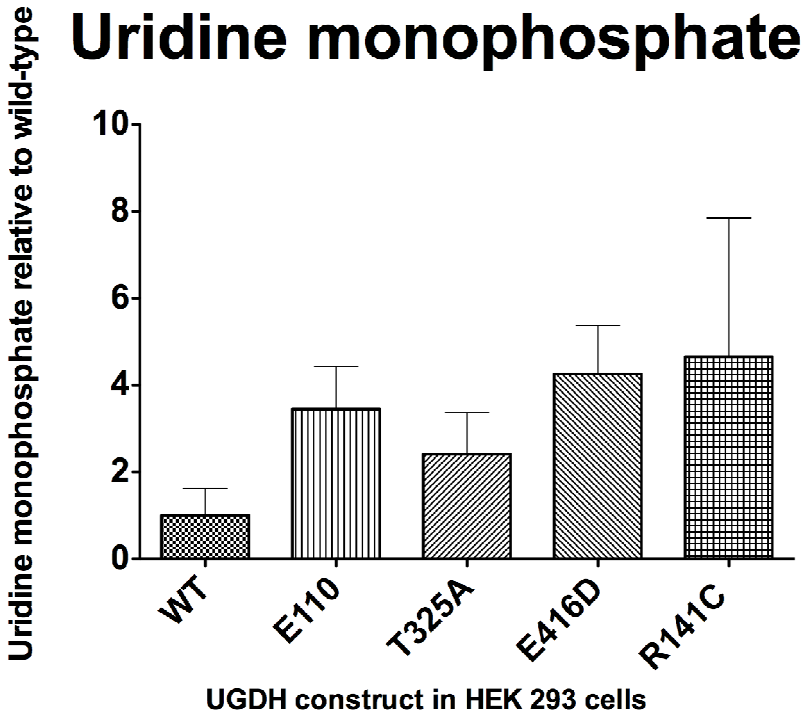

Figure 4.2. Levels of uridine monophosphate in HEK 293 cells. HEK 293 cells were transiently transfected with each construct. Uridine monophosphate levels were measured by HPLC and normalized to total protein levels. Wild-type level is set equal to one for ease of comparison. Error bars represent the SEM of three replicates. Control and GFP values have been omitted.

The two main sources of cellular UMP are *de novo* biosynthesis triggered by low levels of UTP and generation in the ER and Golgi lumen from UDP cleaved from UDP sugars by glycosylation reactions [86, 123-126]. Unlike

other nucleotide triphosphates, a major part of cellular uridine levels is comprised of nucleotide-conjugated sugars [125]. These nucleotide sugars are continually depleted by flux through various metabolic processes. While regeneration of UTP from UDP and UMP is possible, sometimes UTP is depleted to a level that triggers UMP biosynthesis [86, 91, 124].

Further studies are necessary to determine whether the increase in UMP levels observed in the dimeric mutants reflect an impact in *in vivo* UGDH activity due to oligomeric state, as well as a proposed mechanism of any differences. Additionally, the development of new methods to trap UDP-glucuronate before it is utilized are essential to understanding *in vivo* UGDH activity as well as the relative use of UDP-glucuronate by various cellular pathways under distinct cellular conditions.

Therefore, further methods of measuring UGDH activity levels *in vivo* must be developed. One approach would be to block each UDP-glucuronate utilizing pathway and measure UDP-glucuronate levels in the cell. This method would have the advantage of simultaneously informing about the prevalence of UDP-glucuronate flux through each pathway, at least in the cell type chosen for the studies. The studies could then be repeated in cell lines from different tissues and tumors. One example of this type of method that has been previously employed is the use of 4-methylumbelliferone (4-MU), which UGTs use a substrate for glucuronidation [88]. The levels of glucuronidated 4-MU exported to the media can then be measured. The most

obvious target, especially in HEK293 cells, where UGT abundance and glycogen formation are expected to be low, is to block glycosyltransfer reactions in the ER and Golgi lumen. The expected result would be an accumulation of UDP-glucuronate in the cytosol, and, perhaps, differences in UDP-glucuronate levels between wild-type and the dimer mutants might then be detected. Because UDP-glucose is feedback inhibited by UDP-xylose, it might also be necessary and/or informative to block UDP-glucuronate decarboxylase or deplete the UDP-xylose levels of the cytosol in order relieve UGDH inhibition. A recent study in Chinese hamster ovary cells of a mutant defective in UDP-glucuronate decarboxylase measured an increase of over 100 fold in cellular UDP-glucuronate levels [10]. Therefore, blocking one or more UDP-glucuronate pathways, either alone or in combination, will allow us to more accurately measure normal and aberrant *in vivo* UGDH function.

Another promising and related area of inquiry would be to further identify and characterize natural and synthetic inhibitors of UGDH function, both *in vitro* and *in vivo*. The recent screen of a large chemical library conducted for our lab identified a number of inhibitors and activators of UGDH. Interestingly, quercetin and several related molecules were among the inhibitors identified. These inhibitors provide a good starting point for *in vitro* characterizations using our established kinetic assay. Once an informative *in vivo* assay is developed, the most promising inhibitors could be studied in different tissue types for their effect on UGDH function. Thus, there are many productive areas to expand and improve our studies of both

the impacts of oligomeric structure on UGDH function and the further examination of UGDH function and regulation *in vivo*.

Glutamate Cysteine Ligase

Continued examination of the structure and function of glutamate cysteine ligase is essential to understanding the complex active site and catalytic mechanism of this important redox enzyme. In order to do this, two continuing projects are underway: 1. Crystallizing the human holoenzyme and obtaining the structure through x-ray diffraction and 2. Continuing to examine the enzyme active site through site-directed mutagenesis and kinetic studies.

Significant progress was made in crystallizing the human holoenzyme by Katja Biterova, a former member of the lab. She was able to identify conditions and obtain large protein crystals. However, diffraction of these crystals was poor and problems were observed in the cryoprotection process. Thus, further efforts are needed to overcome these limitations and produce crystals that freeze and diffract well.

For the second objective, a set of key catalytic residues has been identified in the GCL active site based on examination of the human homology model and reports in the literature [43, 127]. The following mutants were cloned, expressed, and purified E96Q, K412A, R185L, R426L, and W406F.

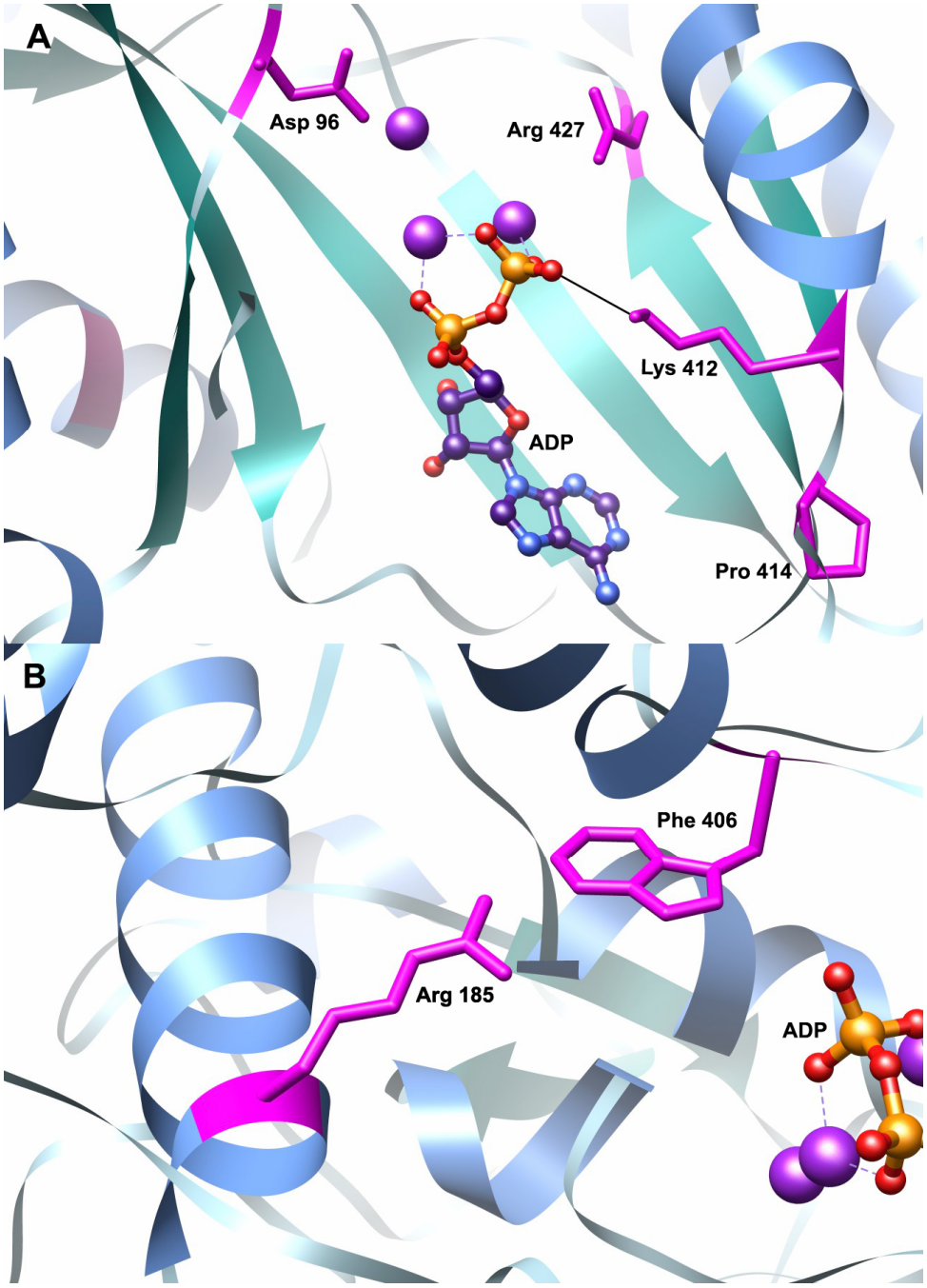

Figure 4.3. Catalytic Residues in GCLC. Key residues in the active site of GCLC are shown in magenta. Magnesium atoms are shown in purple. **Panel A.** Aspartate 427 and glutamate 96 are shown in the magnesium-coordinating region of the active site, while lysine 412 is depicted hydrogen bonding with ADP. Mutation of each of these residues resulted in a catalytically inactive enzyme, in both the GCLC and holoenzyme forms. **Panel B.** Arginine 185 and tryptophan 406 are shown near the proposed cysteine-binding site. Mutation of arginine 185 dramatically increases the amount of cysteine required for activity. Mutation of either residue negatively impacts enzyme catalysis.

An initial kinetic characterization demonstrated that all of the mutant enzymes were catalytically inactive in the catalytic-only form, while R185L and W406F had limited activity in the holoenzyme form. It is not surprising that E96, R427 and L412 are catalytically inactive because E96 and R427 likely participate in magnesium coordination, while L412 likely hydrogen bonds with ATP (Figure 4.3, panel A). Further preliminary characterizations revealed that R185L activity is enhanced in the presence of 25 mM cysteine rather than the usual 1 mM saturating concentration used for this assay, suggesting that R185 may be critical for cysteine coordination in the enzyme active site. Neither mutant appeared to have a significantly altered requirement for glutamate or ATP.

Determination of the apparent kinetic constants of these GCL mutants was planned to coincide with the adaptation of the standard kinetic assay to a high-throughput 96-well plate format. Initial tests of this format with wild-type enzyme showed that similar kinetic constants could be obtained using this format compared to the traditional format. An initial test involving the R185L and W406F mutants demonstrated that the W406F holoenzyme had approximately ¾ the activity of wild-type, while the R185L holoenzyme had only ½ the activity of the holoenzyme. Interestingly, the apparent K_m for glutamate of both mutants was almost identical to that of wild-type.

After determination of the apparent kinetic constants for these two catalytic site mutants, other important residues will be identified for similar studies. For example, the competitive feedback inhibition of glutathione may be examined by mutating residues that might interact with the glycine residue of glutathione that is not present in the product of GCL, □-glutamylcysteine. Thus, while our studies of the GCL clinical mutants yielded critical insights into catalytic function, further structural studies will improve our understanding of this essential redox enzyme.

References

1. Sheehan, D., et al., *Structure, function and evolution of glutathione transferases: implications for classification of non-mammalian members of an ancient enzyme superfamily.* Biochem J, 2001. **360**(Pt 1): p. 1-16.

2. Southwood, H.T., et al., *Carboxylic acid drug-induced DNA nicking in HEK293 cells expressing human UDP-glucuronosyltransferases: role of acyl glucuronide metabolites and glycation pathways.* Chem Res Toxicol, 2007. **20**(10): p. 1520-7.

3. Kochanowski, N., et al., *Intracellular nucleotide and nucleotide sugar contents of cultured CHO cells determined by a fast, sensitive, and high-resolution ion-pair RP-HPLC.* Anal Biochem, 2006. **348**(2): p. 243-51.

4. Grancharov, K., et al., *Natural and synthetic inhibitors of UDP-glucuronosyltransferase.* Pharmacol Ther, 2001. **89**(2): p. 171-86.

5. Rahman, I., J. Marwick, and P. Kirkham, *Redox modulation of chromatin remodeling: impact on histone acetylation and deacetylation, NF-kappaB and pro-inflammatory gene expression.* Biochem Pharmacol, 2004. **68**(6): p. 1255-67.

6. Haddad, J.J. and H.L. Harb, *L-gamma-Glutamyl-L-cysteinyl-glycine (glutathione; GSH) and GSH-related enzymes in the regulation of pro- and anti-inflammatory cytokines: a signaling transcriptional scenario for redox(y) immunologic sensor(s)?* Mol Immunol, 2005. **42**(9): p. 987-1014.

7. Hayes, J.D., J.U. Flanagan, and I.R. Jowsey, *Glutathione transferases.* Annu Rev Pharmacol Toxicol, 2005. **45**: p. 51-88.

8. Egger, S., et al., *UDP-glucose dehydrogenase: structure and function of a potential drug target.* Biochem Soc Trans, 2010. **38**(5): p. 1378-85.

9. Milla, M.E., C.A. Clairmont, and C.B. Hirschberg, *Reconstitution into proteoliposomes and partial purification of the Golgi apparatus membrane UDP-galactose, UDP-xylose, and UDP-glucuronic acid transport activities.* J Biol Chem, 1992. **267**(1): p. 103-7.

10. Bakker, H., et al., *Functional UDP-xylose transport across the endoplasmic reticulum/Golgi membrane in a Chinese hamster ovary cell mutant defective in UDP-xylose Synthase.* J Biol Chem, 2009. **284**(4): p. 2576-83.

11. Hwang, H.Y. and H.R. Horvitz, *The SQV-1 UDP-glucuronic acid decarboxylase and the SQV-7 nucleotide-sugar transporter may act in the Golgi apparatus to affect Caenorhabditis elegans vulval morphogenesis*

and embryonic development. Proc Natl Acad Sci U S A, 2002. **99**(22): p. 14218-23.

12. Moloney, D.J., et al., *Mammalian Notch1 is modified with two unusual forms of O-linked glycosylation found on epidermal growth factor-like modules.* J Biol Chem, 2000. **275**(13): p. 9604-11.

13. Hase, S., et al., *A new trisaccharide sugar chain linked to a serine residue in bovine blood coagulation factors VII and IX.* J Biochem, 1988. **104**(6): p. 867-8.

14. Roden, L. and G. Armand, *Structure of the chondroitin 4-sulfate-protein linkage region. Isolation and characterization of the disaccharide 3-O-beta-D-glucuronosyl-D-galactose.* J Biol Chem, 1966. **241**(1): p. 65-70.

15. Roden, L. and R. Smith, *Structure of the neutral trisaccharide of the chondroitin 4-sulfate-protein linkage region.* J Biol Chem, 1966. **241**(24): p. 5949-54.

16. Franzen, J.S., et al., *Induced versus pre-existing asymmetry models for the half-of-the-sites reactivity effect in bovine liver uridine diphosphoglucose dehydrogenase.* Biochim Biophys Acta, 1980. **614**(2): p. 242-55.

17. Franzen, J.S., R. Ishman, and D.S. Feingold, *Half-of-the-sites reactivity of bovine liver uridine diphosphoglucose dehydrogenase toward iodoacetate and iodoacetamide.* Biochemistry, 1976. **15**(25): p. 5665-71.

18. Franzen, J.S., P.S. Marchetti, and D.S. Feingold, *Resonance energy transfer between catalytic sites of bovine liver uridine diphosphoglucose dehydrogenase.* Biochemistry, 1980. **19**(26): p. 6080-9.

19. Campbell, R.E., et al., *Properties and kinetic analysis of UDP-glucose dehydrogenase from group A streptococci. Irreversible inhibition by UDP-chloroacetol.* J Biol Chem, 1997. **272**(6): p. 3416-22.

20. Easley, K.E., et al., *Characterization of human UDP-glucose dehydrogenase reveals critical catalytic roles for lysine 220 and aspartate 280.* Biochemistry, 2007. **46**(2): p. 369-78.

21. Ridley, W.P., J.P. Houchins, and S. Kirkwood, *Mechanism of action of uridine diphosphoglucose dehydrogenase. Evidence for a second reversible dehydrogenation step involving an essential thiol group.* J Biol Chem, 1975. **250**(22): p. 8761-7.

22. Sommer, B.J., J.J. Barycki, and M.A. Simpson, *Characterization of human UDP-glucose dehydrogenase. CYS-276 is required for the second of two successive oxidations.* J Biol Chem, 2004. **279**(22): p. 23590-6.

23. Ge, X., et al., *Active site residues and mechanism of UDP-glucose dehydrogenase.* Eur J Biochem, 2004. **271**(1): p. 14-22.

24. Lapointe, J. and C. Labrie, *Identification and cloning of a novel androgen-responsive gene, uridine diphosphoglucose dehydrogenase, in human breast cancer cells.* Endocrinology, 1999. **140**(10): p. 4486-93.

25. Nelson, P.S., et al., *The program of androgen-responsive genes in neoplastic prostate epithelium.* Proc Natl Acad Sci U S A, 2002. **99**(18): p. 11890-5.

26. Wei, Q., et al., *Androgen-stimulated UDP-glucose dehydrogenase expression limits prostate androgen availability without impacting hyaluronan levels.* Cancer Res, 2009. **69**(6): p. 2332-9.

27. Vatsyayan, J., et al., *Identification of a cis-acting element responsible for negative regulation of the human UDP-glucose dehydrogenase gene expression.* Biosci Biotechnol Biochem, 2006. **70**(2): p. 401-10.

28. Vatsyayan, J., S.J. Lee, and H.Y. Chang, *Effects of xenobiotics and peroxisome proliferator-activated receptor-alpha on the human UDPglucose dehydrogenase gene expression.* J Biochem Mol Toxicol, 2005. **19**(5): p. 279-88.

29. De Luca, G., et al., *Effect of some nucleotides on the regulation of glycosaminoglycan biosynthesis.* Connect Tissue Res, 1976. **4**(4): p. 247-54.

30. Hwang, E.Y., et al., *Inhibitory effects of gallic acid and quercetin on UDP-glucose dehydrogenase activity.* FEBS Lett, 2008. **582**(27): p. 3793-7.

31. Knudson, W., et al., *The role and regulation of tumour-associated hyaluronan.* Ciba Found Symp, 1989. **143**: p. 150-9; discussion 159-69, 281-5.

32. Herman, T. and H.R. Horvitz, *Three proteins involved in Caenorhabditis elegans vulval invagination are similar to components of a glycosylation pathway.* Proc Natl Acad Sci U S A, 1999. **96**(3): p. 974-9.

33. Herman, T., E. Hartwieg, and H.R. Horvitz, *sqv mutants of Caenorhabditis elegans are defective in vulval epithelial invagination.* Proc Natl Acad Sci U S A, 1999. **96**(3): p. 968-73.

34. Hwang, H.Y. and H.R. Horvitz, *The Caenorhabditis elegans vulval morphogenesis gene sqv-4 encodes a UDP-glucose dehydrogenase that is temporally and spatially regulated.* Proc Natl Acad Sci U S A, 2002. **99**(22): p. 14224-9.

35. Walsh, E.C. and D.Y. Stainier, *UDP-glucose dehydrogenase required for cardiac valve formation in zebrafish.* Science, 2001. **293**(5535): p. 1670-3.

36. Hayes, J.D. and D.J. Pulford, *The glutathione S-transferase supergene family: regulation of GST and the contribution of the isoenzymes to cancer chemoprotection and drug resistance.* Crit Rev Biochem Mol Biol, 1995. **30**(6): p. 445-600.

37. Griffith, O.W. and R.T. Mulcahy, *The enzymes of glutathione synthesis: gamma-glutamylcysteine synthetase.* Adv Enzymol Relat Areas Mol Biol, 1999. **73**: p. 209-67, xii.

38. Tateishi, N., et al., *Rat liver glutathione: possible role as a reservoir of cysteine.* J Nutr, 1977. **107**(1): p. 51-60.

39. Dickinson, D.A. and H.J. Forman, *Glutathione in defense and signaling: lessons from a small thiol.* Ann N Y Acad Sci, 2002. **973**: p. 488-504.

40. Huang, C.S., M.E. Anderson, and A. Meister, *Amino acid sequence and function of the light subunit of rat kidney gamma-glutamylcysteine synthetase.* J Biol Chem, 1993. **268**(27): p. 20578-83.

41. Huang, C.S., et al., *Catalytic and regulatory properties of the heavy subunit of rat kidney gamma-glutamylcysteine synthetase.* J Biol Chem, 1993. **268**(26): p. 19675-80.

42. Richman, P.G. and A. Meister, *Regulation of gamma-glutamyl-cysteine synthetase by nonallosteric feedback inhibition by glutathione.* J Biol Chem, 1975. **250**(4): p. 1422-6.

43. Abbott, J.J., J.L. Ford, and M.A. Phillips, *Substrate binding determinants of Trypanosoma brucei gamma-glutamylcysteine synthetase.* Biochemistry, 2002. **41**(8): p. 2741-50.

44. Biterova, E.I. and J.J. Barycki, *Mechanistic details of glutathione biosynthesis revealed by crystal structures of Saccharomyces cerevisiae glutamate cysteine ligase.* J Biol Chem, 2009. **284**(47): p. 32700-8.

45. Copley, S.D. and J.K. Dhillon, *Lateral gene transfer and parallel evolution in the history of glutathione biosynthesis genes.* Genome Biol, 2002. **3**(5): p. research0025.

46. Hibi, T., et al., *Crystal structure of gamma-glutamylcysteine synthetase: insights into the mechanism of catalysis by a key enzyme for glutathione homeostasis.* Proc Natl Acad Sci U S A, 2004. **101**(42): p. 15052-7.

47. Hothorn, M., et al., *Structural basis for the redox control of plant glutamate cysteine ligase.* J Biol Chem, 2006. **281**(37): p. 27557-65.

48. Matte, A., L.W. Tari, and L.T. Delbaere, *How do kinases transfer phosphoryl groups?* Structure, 1998. **6**(4): p. 413-9.

49. Jez, J.M., R.E. Cahoon, and S. Chen, *Arabidopsis thaliana glutamate-cysteine ligase: functional properties, kinetic mechanism, and regulation of activity.* J Biol Chem, 2004. **279**(32): p. 33463-70.

50. Yip, B. and F.B. Rudolph, *The kinetic mechanism of rat kidney gamma-glutamylcysteine synthetase.* J Biol Chem, 1976. **251**(12): p. 3563-8.

51. Franklin, C.C., et al., *Structure, function, and post-translational regulation of the catalytic and modifier subunits of glutamate cysteine ligase.* Mol Aspects Med, 2009. **30**(1-2): p. 86-98.

52. Chen, Y., et al., *Hepatocyte-specific Gclc deletion leads to rapid onset of steatosis with mitochondrial injury and liver failure.* Hepatology, 2007. **45**(5): p. 1118-28.

53. Krzywanski, D.M., et al., *Variable regulation of glutamate cysteine ligase subunit proteins affects glutathione biosynthesis in response to oxidative stress.* Arch Biochem Biophys, 2004. **423**(1): p. 116-25.

54. Lee, J.I., J. Kang, and M.H. Stipanuk, *Differential regulation of glutamate-cysteine ligase subunit expression and increased holoenzyme formation in response to cysteine deprivation.* Biochem J, 2006. **393**(Pt 1): p. 181-90.

55. Tu, Z. and M.W. Anders, *Identification of an important cysteine residue in human glutamate-cysteine ligase catalytic subunit by site-directed mutagenesis.* Biochem J, 1998. **336 (Pt 3)**: p. 675-80.

56. Fraser, J.A., et al., *The modifier subunit of Drosophila glutamate-cysteine ligase regulates catalytic activity by covalent and noncovalent interactions and influences glutathione homeostasis in vivo.* J Biol Chem, 2003. **278**(47): p. 46369-77.

57. Ochi, T., *Hydrogen peroxide increases the activity of gamma-glutamylcysteine synthetase in cultured Chinese hamster V79 cells.* Arch Toxicol, 1995. **70**(2): p. 96-103.

58. Ochi, T., *Menadione causes increases in the level of glutathione and in the activity of gamma-glutamylcysteine synthetase in cultured Chinese hamster V79 cells.* Toxicology, 1996. **112**(1): p. 45-55.

59. Sierra-Rivera, E., et al., *Assignment of the gene (GLCLC) that encodes the heavy subunit of gamma-glutamylcysteine synthetase to human chromosome 6.* Cytogenet Cell Genet, 1995. **70**(3-4): p. 278-9.

60. Tsuchiya, K., et al., *Mapping of the glutamate-cysteine ligase catalytic subunit gene (GLCLC) to human chromosome 6p12 and mouse chromosome 9D-E and of the regulatory subunit gene (GLCLR) to human chromosome 1p21-p22 and mouse chromosome 3H1-3.* Genomics, 1995. **30**(3): p. 630-2.

61. Gipp, J.J., H.H. Bailey, and R.T. Mulcahy, *Cloning and sequencing of the cDNA for the light subunit of human liver gamma-glutamylcysteine synthetase and relative mRNA levels for heavy and light subunits in human normal tissues.* Biochem Biophys Res Commun, 1995. **206**(2): p. 584-9.

62. Lu, S.C., *Regulation of glutathione synthesis.* Mol Aspects Med, 2009. **30**(1-2): p. 42-59.

63. Griffith, O.W. and A. Meister, *Glutathione: interorgan translocation, turnover, and metabolism.* Proc Natl Acad Sci U S A, 1979. **76**(11): p. 5606-10.

64. Dalton, T.P., et al., *Knockout of the mouse glutamate cysteine ligase catalytic subunit (Gclc) gene: embryonic lethal when homozygous, and proposed model for moderate glutathione deficiency when heterozygous.* Biochem Biophys Res Commun, 2000. **279**(2): p. 324-9.

65. Beutler, E., et al., *The molecular basis of a case of gamma-glutamylcysteine synthetase deficiency.* Blood, 1999. **94**(8): p. 2890-4.

66. Hamilton, D., et al., *A novel missense mutation in the gamma-glutamylcysteine synthetase catalytic subunit gene causes both decreased enzymatic activity and glutathione production.* Blood, 2003. **102**(2): p. 725-30.

67. Hirono, A., et al., *Three cases of hereditary nonspherocytic hemolytic anemia associated with red blood cell glutathione deficiency.* Blood, 1996. **87**(5): p. 2071-4.

68. Manu Pereira, M., et al., *Chronic non-spherocytic hemolytic anemia associated with severe neurological disease due to gamma-glutamylcysteine synthetase deficiency in a patient of Moroccan origin.* Haematologica, 2007. **92**(11): p. e102-5.

69. Ristoff, E., et al., *A missense mutation in the heavy subunit of gamma-glutamylcysteine synthetase gene causes hemolytic anemia.* Blood, 2000. **95**(7): p. 2193-6.

70. Aaltomaa, S., et al., *Strong Stromal Hyaluronan Expression Is Associated with PSA Recurrence in Local Prostate Cancer.* Urol Int, 2002. **69**(4): p. 266-72.

71. Anttila, M.A., et al., *High levels of stromal hyaluronan predict poor disease outcome in epithelial ovarian cancer.* Cancer Res, 2000. **60**(1): p. 150-5.

72. Auvinen, P., et al., *Hyaluronan in peritumoral stroma and malignant cells associates with breast cancer spreading and predicts survival.* Am J Pathol, 2000. **156**(2): p. 529-36.

73. Ropponen, K., et al., *Tumor cell-associated hyaluronan as an unfavorable prognostic factor in colorectal cancer.* Cancer Res, 1998. **58**(2): p. 342-7.

74. Stern, R., *Hyaluronidases in cancer biology.* Semin Cancer Biol, 2008. **18**(4): p. 275-80.

75. Tammi, R.H., et al., *Hyaluronan in human tumors: pathobiological and prognostic messages from cell-associated and stromal hyaluronan.* Semin Cancer Biol, 2008. **18**(4): p. 288-95.

76. Toole, B.P. and V.C. Hascall, *Hyaluronan and tumor growth.* Am J Pathol, 2002. **161**(3): p. 745-7.

77. Huang, D., et al., *Udp-glucose dehydrogenase as a novel field-specific candidate biomarker of prostate cancer.* Int J Cancer, 2010. **126**(2): p. 315-27.

78. Ordman, A.B. and S. Kirkwood, *Mechanism of action of uridine diphoglucose dehydrogenase. Evidence for an essential lysine residue at the active site.* J Biol Chem, 1977. **252**(4): p. 1320-6.

79. Ordman, A.B. and S. Kirkwood, *UDPglucose dehydrogenase. Kinetics and their mechanistic implications.* Biochim Biophys Acta, 1977. **481**(1): p. 25-32.

80. Smith, K.A., et al., *Dominant-negative ALK2 allele associates with congenital heart defects.* Circulation, 2009. **119**(24): p. 3062-9.

81. Schuck, P., *On the analysis of protein self-association by sedimentation velocity analytical ultracentrifugation.* Anal Biochem, 2003. **320**(1): p. 104-24.

82. Bradford, M.M., *A rapid and sensitive method for the quantitation of microgram quantities of protein utilizing the principle of protein-dye binding.* Anal Biochem, 1976. **72**: p. 248-54.

83. Linster, C.L. and E. Van Schaftingen, *Rapid stimulation of free glucuronate formation by non-glucuronidable xenobiotics in isolated rat hepatocytes.* J Biol Chem, 2003. **278**(38): p. 36328-33.

84. Reiss, P.D., P.F. Zuurendonk, and R.L. Veech, *Measurement of tissue purine, pyrimidine, and other nucleotides by radial compression high-performance liquid chromatography.* Anal Biochem, 1984. **140**(1): p. 162-71.

85. Gessner, T., A. Jacknowitz, and C.A. Vollmer, *Studies of mammalian glucoside conjugation.* Biochem J, 1973. **132**(2): p. 249-58.

86. Keppler, D.O., et al., *Uridylate trapping, induction of UTP deficiency, and stimulation of pyrimidine synthesis de novo by D-galactosone.* Biochem J, 1982. **206**(1): p. 139-46.

87. Weckbecker, G. and D.O. Keppler, *Separation and analysis of 4'-epimeric UDP-sugars by borate high-performance liquid chromatography.* Anal Biochem, 1983. **132**(2): p. 405-12.

88. Kultti, A., et al., *4-Methylumbelliferone inhibits hyaluronan synthesis by depletion of cellular UDP-glucuronic acid and downregulation of hyaluronan synthase 2 and 3.* Exp Cell Res, 2009. **315**(11): p. 1914-23.

89. Haugaard, E.S., K.B. Frantz, and N. Haugaard, *Effect of uridine on cellular UTP and glycogen synthesis in skeletal muscle: stimulation of UTP formation by insulin.* Proc Natl Acad Sci U S A, 1977. **74**(6): p. 2339-42.

90. Evans, D.R. and H.I. Guy, *Mammalian pyrimidine biosynthesis: fresh insights into an ancient pathway.* J Biol Chem, 2004. **279**(32): p. 33035-8.

91. Lecca, D. and S. Ceruti, *Uracil nucleotides: from metabolic intermediates to neuroprotection and neuroinflammation.* Biochem Pharmacol, 2008. **75**(10): p. 1869-81.

92. Hebert, D.N., S.C. Garman, and M. Molinari, *The glycan code of the endoplasmic reticulum: asparagine-linked carbohydrates as protein maturation and quality-control tags.* Trends Cell Biol, 2005. **15**(7): p. 364-70.

93. Chambers, J.K., et al., *A G protein-coupled receptor for UDP-glucose.* J Biol Chem, 2000. **275**(15): p. 10767-71.

94. Abbracchio, M.P., et al., *Characterization of the UDP-glucose receptor (re-named here the P2Y14 receptor) adds diversity to the P2Y receptor family.* Trends Pharmacol Sci, 2003. **24**(2): p. 52-5.

95. Lazarowski, E.R., et al., *Release of cellular UDP-glucose as a potential extracellular signaling molecule.* Mol Pharmacol, 2003. **63**(5): p. 1190-7.

96. Lazarowski, E.R., R.C. Boucher, and T.K. Harden, *Mechanisms of release of nucleotides and integration of their action as P2X- and P2Y-receptor activating molecules.* Mol Pharmacol, 2003. **64**(4): p. 785-95.

97. Muraoka, M., et al., *Variety of nucleotide sugar transporters with respect to the interaction with nucleoside mono- and diphosphates.* J Biol Chem, 2007. **282**(34): p. 24615-22.

98. Burchell, B., *Substrate specificity and properties of uridine diphosphate glucuronyltransferase purified to apparent homogeneity from phenobarbital-treated rat liver.* Biochem J, 1978. **173**(3): p. 749-57.

99. Roy Chowdhury, J., et al., *Isolation and characterization of multiple forms of rat liver UDP-glucuronate glucuronosyltransferase.* Biochem J, 1986. **233**(3): p. 827-37.

100. Fujiwara, R., et al., *Key amino acid residues responsible for the differences in substrate specificity of human UDP-glucuronosyltransferase (UGT)1A9 and UGT1A8.* Drug Metab Dispos, 2009. **37**(1): p. 41-6.

101. Lieberman, M.W., et al., *Growth retardation and cysteine deficiency in gamma-glutamyl transpeptidase-deficient mice.* Proc Natl Acad Sci U S A, 1996. **93**(15): p. 7923-6.

102. Wang, W. and N. Ballatori, *Endogenous glutathione conjugates: occurrence and biological functions.* Pharmacol Rev, 1998. **50**(3): p. 335-56.

103. Shi, Z.Z., et al., *Mutations in the glutathione synthetase gene cause 5-oxoprolinuria.* Nat Genet, 1996. **14**(3): p. 361-5.

104. Yang, Y., et al., *Initial characterization of the glutamate-cysteine ligase modifier subunit Gclm(-/-) knockout mouse. Novel model system for a severely compromised oxidative stress response.* J Biol Chem, 2002. **277**(51): p. 49446-52.

105. Shi, Z.Z., et al., *Glutathione synthesis is essential for mouse development but not for cell growth in culture.* Proc Natl Acad Sci U S A, 2000. **97**(10): p. 5101-6.

106. Townsend, D.M., K.D. Tew, and H. Tapiero, *The importance of glutathione in human disease.* Biomed Pharmacother, 2003. **57**(3-4): p. 145-55.

107. Reid, M. and F. Jahoor, *Glutathione in disease.* Curr Opin Clin Nutr Metab Care, 2001. **4**(1): p. 65-71.

108. Meister, A. and M.E. Anderson, *Glutathione.* Annu Rev Biochem, 1983. **52**: p. 711-60.

109. Mumberg, D., R. Muller, and M. Funk, *Yeast vectors for the controlled expression of heterologous proteins in different genetic backgrounds.* Gene, 1995. **156**(1): p. 119-22.

110. Eyer, P. and D. Podhradsky, *Evaluation of the micromethod for determination of glutathione using enzymatic cycling and Ellman's reagent.* Anal Biochem, 1986. **153**(1): p. 57-66.

111. Gietz, R.D., et al., *Studies on the transformation of intact yeast cells by the LiAc/SS-DNA/PEG procedure.* Yeast, 1995. **11**(4): p. 355-60.

112. Biterova, E.I. and J.J. Barycki, *Structural basis for feedback and pharmacological inhibition of Saccharomyces cerevisiae glutamate cysteine ligase.* J Biol Chem, 2010. **285**(19): p. 14459-66.

113. Sun, W.M., Z.Z. Huang, and S.C. Lu, *Regulation of gamma-glutamylcysteine synthetase by protein phosphorylation.* Biochem J, 1996. **320 (Pt 1)**: p. 321-8.

114. Yan, N. and A. Meister, *Amino acid sequence of rat kidney gamma-glutamylcysteine synthetase.* J Biol Chem, 1990. **265**(3): p. 1588-93.

115. Backos, D.S., et al., *Posttranslational modification and regulation of glutamate-cysteine ligase by the alpha,beta-unsaturated aldehyde 4-hydroxy-2-nonenal.* Free Radic Biol Med, 2011. **50**(1): p. 14-26.

116. Chen, Y., et al., *Glutamate cysteine ligase catalysis: dependence on ATP and modifier subunit for regulation of tissue glutathione levels.* J Biol Chem, 2005. **280**(40): p. 33766-74.

117. Ohtake, Y. and S. Yabuuchi, *Molecular cloning of the gamma-glutamylcysteine synthetase gene of Saccharomyces cerevisiae.* Yeast, 1991. **7**(9): p. 953-61.

118. Spector, D., J. Labarre, and M.B. Toledano, *A genetic investigation of the essential role of glutathione: mutations in the proline biosynthesis*

pathway are the only suppressors of glutathione auxotrophy in yeast. J Biol Chem, 2001. **276**(10): p. 7011-6.

119. Tu, Z. and M.W. Anders, *Expression and characterization of human glutamate-cysteine ligase.* Arch Biochem Biophys, 1998. **354**(2): p. 247-54.

120. Fraser, J.A., R.D. Saunders, and L.I. McLellan, *Drosophila melanogaster glutamate-cysteine ligase activity is regulated by a modifier subunit with a mechanism of action similar to that of the mammalian form.* J Biol Chem, 2002. **277**(2): p. 1158-65.

121. Yang, Y., et al., *Interaction between the catalytic and modifier subunits of glutamate-cysteine ligase.* Biochem Pharmacol, 2007. **74**(2): p. 372-81.

122. D'Alessandro, A., P.G. Righetti, and L. Zolla, *The red blood cell proteome and interactome: an update.* J Proteome Res, 2010. **9**(1): p. 144-63.

123. Plagemann, P.G., *Nucleotide pools in Novikoff rat hepatoma cells growing in suspension culture. 3. Effects of nucleosides in medium on levels of nucleotides in separate nucleotide pools for nuclear and cytoplasmic RNA synthesis.* J Cell Biol, 1972. **52**(1): p. 131-46.

124. Kim, M.K., et al., *Higher intracellular levels of uridinemonophosphate under nitrogen-limited conditions enhance metabolic flux of curdlan synthesis in Agrobacterium species.* Biotechnol Bioeng, 1999. **62**(3): p. 317-23.

125. Jones, M.E., *Pyrimidine nucleotide biosynthesis in animals: genes, enzymes, and regulation of UMP biosynthesis.* Annu Rev Biochem, 1980. **49**: p. 253-79.

126. Pausch, J., et al., *Control of pyrimidine biosynthesis in the perfused liver. Feedback inhibition of glutamine-dependent carbamoyl phosphate synthetase.* Eur J Biochem, 1975. **53**(2): p. 349-56.

127. Abbott, J.J., et al., *Structure prediction and active site analysis of the metal binding determinants in gamma -glutamylcysteine synthetase.* J Biol Chem, 2001. **276**(45): p. 42099-107.